

Seasonal variation of the Hough modes of the diurnal component of ozone heating evaluated from Aura Microwave Limb Sounder observations

Jiyao Xu,¹ A. K. Smith,² Guoying Jiang,¹ and Wei Yuan¹

Received 10 September 2009; revised 28 December 2009; accepted 4 January 2010; published 26 May 2010.

[1] The global distribution of atmospheric ozone from August 2004 to December 2008 observed by Aura Microwave Limb Sounder is used to calculate the daily ozone heating rate. Comparison with a photochemical model shows that the Strobel/Zhu parameterized model of the solar heating rate gives an accurate diurnal cycle of the heating in the 10–70 km altitude range. The heating calculated using the Strobel/Zhu model is decomposed into Hough modes and the annual (AO), semiannual (SAO), and quasi-biennial (QBO) periodicities of each Hough mode are presented. The results show that the majority of the O₃ heating goes into the symmetric (1,–2), (1,1), and (1,–4) modes. The largest propagating mode (1,1) and the largest trapped mode (1,–2) have obvious SAO signatures near 47 km, where the heating magnitude is largest. The forcing of the propagating (1,1) mode by ozone heating is larger during solstices than during equinoxes. There are also AO in the (1,–2) and (1,1) modes. The QBO signatures are relatively weak in the two modes in the region of large heating rate. The heating rate of the strongest propagating mode (1,1) reaches maximum near December/January solstice; that for the strongest trapped mode (1,–2) reaches maximum near equinoxes. The strongest annual variation takes place in the (1,–1) mode; it reaches 3.6 K/d near 45 km at the December/January solstice. A new parameterization of the diurnal component of the heating rate, which covers the vertical range from 10 km to 70 km, is developed based on the seasonal variations in each Hough mode.

Citation: Xu, J., A. K. Smith, G. Jiang, and W. Yuan (2010), Seasonal variation of the Hough modes of the diurnal component of ozone heating evaluated from Aura Microwave Limb Sounder observations, *J. Geophys. Res.*, **115**, D10110, doi:10.1029/2009JD013179.

1. Introduction

[2] The atmospheric heating caused by the absorption of solar radiation by ozone and molecular oxygen is important in forcing the circulation and tides in the stratosphere, mesosphere, and lower thermosphere. The heating varies seasonally due to variations in the solar zenith angle and in the Earth–Sun distance. The heating can also vary due to changes in the amount and vertical structure of middle atmosphere ozone.

[3] Several parameterized heating rates have been developed for use with numerical models or observations. *Lacis and Hansen* [1974] developed a parameterization for ozone absorption. *Strobel* [1978] developed a parameterized model for calculating the ozone and O₂ heating rates in the range 15–120 km. *Zhu* [1994] made improvements to this parameterization. *Brasseur and Offermann* [1986] and

Mlynczak and Solomon [1993] evaluated the energy budget in the mesopause region. Their results show that heating by exothermic chemical reaction is a dominant contributor to the heating rate, especially near the mesopause at night.

[4] The atmospheric tides are forced by diurnally varying heating, including the heating from water vapor in the troposphere, ozone heating in the middle atmosphere, and O₂ heating in the middle atmosphere and lower thermosphere [e.g., *Hagan*, 1996]. The importance of these sources for tides points to the need for a realistic parameterization of the structure and variations of the heating.

[5] *Forbes and Garrett* [1978] used the U. S. Standard Atmosphere (1976) midlatitude ozone model in a computation of the ozone and water vapor heating rates as functions of height, latitude, and local time during equinox and solstice. They also decomposed the heating rate into Fourier harmonics of a solar day (i.e., periods of 24, 12, and 8 h) and, further, into Hough modes. In the calculation, they used a single profile (uniform in latitude) for the ozone distribution. They found significant structural and seasonal differences from the ozone heating distribution presented by *Chapman and Lindzen* [1970]. The ozone heating rates they calculated were used for modeling the diurnal tide

¹State Key Laboratory of Space Weather, Center for Space Science and Applied Research, Chinese Academy of Sciences, Beijing, China.

²Atmospheric Chemistry Division, National Center for Atmospheric Research, Boulder, CO, USA.

[Forbes, 1982]. Groves [1982] calculated the diurnal and semidiurnal components of ozone heating, decomposed into Hough modes, for four midseason months (January, April, July and October) based on the limited ground-based and satellite observational ozone data available at the time. In the ozone data set he used, observations are sparse at high latitudes and above 50 km. The latitudinal and vertical dependences were obtained by a polynomial fit.

[6] Since then, there has been an enormous increase in our knowledge of middle atmosphere ozone due to extensive ozone observations made by satellite. For instance, SAGE II (Stratospheric Aerosol and Gas Experiment II), which was launched in October 1984 aboard the Earth Radiation Budget Satellite (ERBS), used the solar occultation technique to retrieve 15 sunrise and sunset observations of stratospheric ozone each day [e.g., Cunnold *et al.*, 1989]. The Upper Atmosphere Research Satellite (UARS) was launched in September, 1991 carried several instruments that measured middle atmosphere ozone. The Halogen Occultation Experiment (HALOE) used solar occultation to made 15 daily sunrise and sunset observations of the vertical profiles of ozone and other chemical species [Russell *et al.*, 1993]. The solar occultation technique results in profile measurements that have a limited local time range and observe a very narrow range of latitudes during each day. Both of these limit the utility of this type of data for obtaining global maps over the range of sunlight conditions. Sunrise and sunset can be particularly problematic because rapid variations can occur in the ozone density, especially above 50 km. Another UARS instrument, the Microwave Limb Sounder (MLS), also made observations of stratospheric ozone. However, after 15 March 1994 the measurements became increasingly sparse in order to conserve the lifetime of the MLS antenna scan mechanism and UARS power.

[7] More recently, satellite observations have become available that include both the stratosphere and mesosphere (e.g., TIMED/SABER, Envisat/MIPAS, and Aura/MLS). SABER (Sounding of the Atmosphere using Broadband Emission Radiometry) on the TIMED (Thermosphere, Ionosphere, Mesosphere, Energetics and Dynamics) satellite, which was launched in December 2001, began making observations of the global ozone distribution in the stratosphere and mesosphere in late January, 2002. The TIMED orbit precesses slowly so it takes more than 60 days to complete a full 24 h coverage of local time. TIMED/SABER gives ozone data from 53° in one hemisphere to 83° in the other; about every about 60 days it yaws to face the other hemisphere. Since high latitudes (poleward of 53) are sampled only on alternate yaw cycles, the time series of ozone and other products at these latitudes have repeated 60 day gaps in coverage. The incomplete latitudinal coverage limits the application of TIMED/SABER ozone for truly global analysis.

[8] A new generation MLS instrument on the Aura satellite has been providing continuous observations of the near-global (82°S to 82°N) distributions of several atmospheric parameters, including temperature and ozone, extending from 10 km to above 70 km in height, since August 2004. The near-global coverage and multiyear duration make these data particularly useful for determining the heating rate. This is a good opportunity to investigate the

details of the structure and seasonal variation of the ozone heating rate and its tidal components. The purpose of this paper is to use ozone data from Aura/MLS to evaluate the diurnal component of the ozone heating rate and discuss its seasonal variation. A new parameterized representation of the diurnal component in the heating rate decomposed into Hough modes is developed.

[9] The paper is organized as follows. Section 2 discusses the method for calculating the atmospheric heating rate and its harmonic components and evaluates the correctness of the heating parameterization. The calculation of the ozone heating rate using Aura/MLS data and its decomposition into Hough modes are described in section 3. In section 4, we discuss the features of the seasonal and interannual variations in the diurnal Hough components of the heating rate. In section 5, a new parameterization of the diurnal component in the atmospheric heating rate in the middle and lower thermosphere is developed and evaluated. A summary is given in section 6.

2. Evaluation of the Parameterized Heating Rate and Its Harmonic Components

[10] In the middle atmosphere, the dominant atmospheric heating process is due to the absorption of solar radiation by ozone in the Hartley, Huggins, and Chappius bands. In the upper mesosphere and lower thermosphere, O₂ absorption of solar UV radiation in the Schumann-Runge bands and continuum becomes dominant. Strobel [1978] calculated coefficients for a parameterization of the heating rate calculation that uses vertical profiles of ozone and O₂ and the solar zenith angle. Zhu [1994] made improvement on this parameterization. In this paper, we refer to this heating parameterization as the Strobel/Zhu model. One shortcoming of this approach is that the parameterization can only represent the heating from absorbed ultraviolet energy, not that from other photochemical processes. Mlynarczyk and Solomon [1993] showed that, in the mesopause region, heating from exothermic chemical reactions between oxygen and hydrogen compounds makes a large contribution on the heating rate, especially during night. In effect, the chemical heating processes redistribute some of the heating from the day, when absorption occurs, to the night. The energy can also be spread to other parts of the atmosphere if transport of photodissociation products occurs before the energy is released as heat. The Strobel/Zhu model can separate out that part of the heating that goes into photodissociation but, without additional information such as a chemical model, cannot determine the eventual heat produced when exothermic reactions occur.

[11] In this section, we evaluate the vertical range over which the Strobel/Zhu parameterization of the heating rates is reliable. We calculate the heating rate by using a time-dependent 1-D photochemical model [Xu *et al.*, 2000, 2003] that accounts for the variation of solar zenith angle during daylight hours. The model calculates 16 species belonging to the oxygen (O₃, O(³P), O(¹D)), hydrogen (H, OH, HO₂), nitrogen (N, NO, NO₂, NO₃, N₂O₅, HNO₃) and chlorine (Cl, ClO, HCl, HOCl) families. Concentrations of longer-lived species are specified. In the model, the heating rate q is calculated directly using all the photochemical reactions of the four chemical families listed above, similar to the cal-

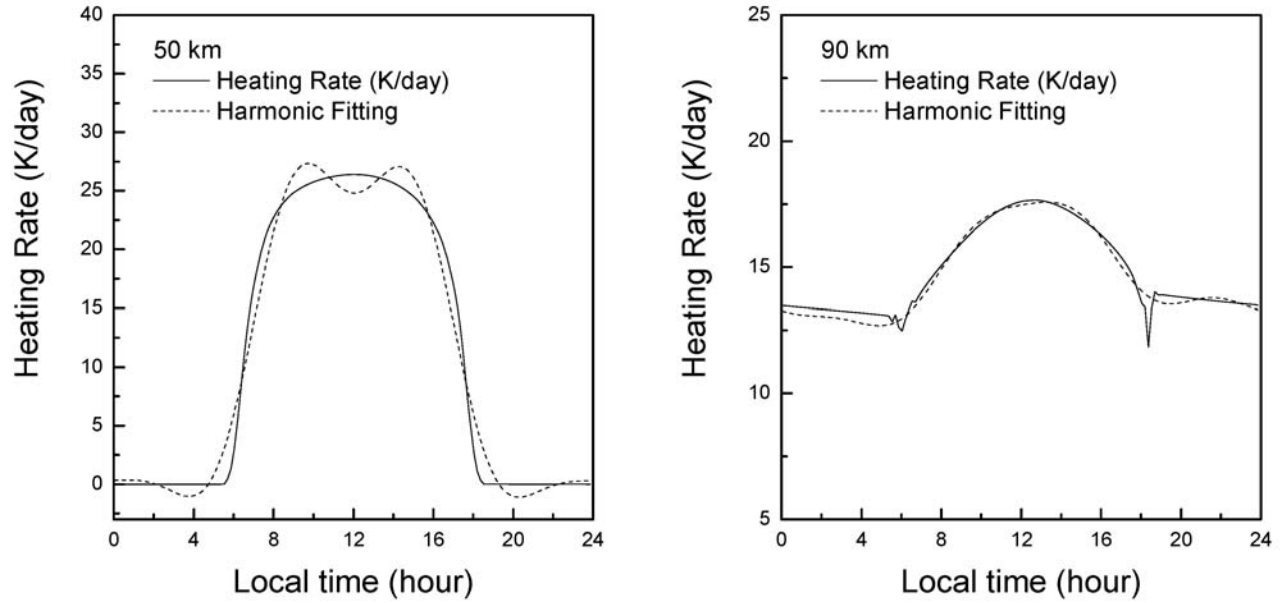


Figure 1. The diurnal variation of the heating rate at (left) 50 km and (right) 90 km. Solid line is the model calculation; dashed line is harmonic fitting.

calculation methods described by *Brasseur and Offermann* [1986] and *Mlynczak and Solomon* [1993]. That part of the absorbed solar energy in the model that leads to photodissociation is assumed not to contribute to the heating until the heat is released by an exothermic reaction. The heating rate therefore includes two parts: (1) the excess contribution from solar ultraviolet absorption that is converted immediately to heat q_s and (2) the heat released during exothermic chemical reactions q_c . The model does not simulate a mean circulation and therefore neglects transport of trace species.

[12] The net photochemical heating rate is

$$q = q_s + q_c - e_R, \quad (1)$$

where e_R is the energy lost by radiative airglow emissions. The significant reduction of the heating efficiency above the stratopause due to energy radiated by excited photolysis products and by excited products of exothermic chemical reactions (airglow) was quantified by *Mlynczak and Solomon* [1993]. They calculated the efficiencies of several important absorption bands and chemical reactions and determined the bulk efficiencies that combine effects of the deposition of solar ultraviolet radiation and the release of energy through exothermic chemical reactions. They found that airglow and chemiluminescence result in about a 15–25% loss in the mesopause region. At and below about 50 km, the efficiency is close to unity (near 0% loss). By using the bulk solar and chemical heating efficiency [*Mlynczak and Solomon*, 1993], equation (1) becomes

$$q = \varepsilon(q_s + q_c). \quad (2)$$

We take the bulk solar and chemical heating efficiency from *Xu et al.* [2003, equation (10)] in the calculations.

[13] Figure 1 gives the diurnal variation of the heating rate at 50 and 90 km at the equator calculated by the 1-D model (solid lines). At 50 km, the heating follows the solar zenith angle and ozone optical depth, indicating that the absorbed solar ultraviolet radiation is converted immediately and completely to heat. However, at 90 km, not all of the absorbed solar energy immediately appears as heat in the atmosphere. Substantial portions of the incident solar energy are stored as chemical potential energy (i.e., as photodissociation products or other reactant species) and released as heat during exothermic reactions, which can take place during day or night.

[14] The harmonic components of the heating rate, which include the daily mean and the 24 h, 12 h, 8 h and 6 h periodicities, at day number d , altitude z , and latitude θ are calculated as follows:

$$q(d, \theta, z, t) = Q_0(d, \theta, z) + \sum_{m=1}^4 [Q_m^c(d, \theta, z) \cos(m\omega_0 t) + Q_m^s(d, \theta, z) \sin(m\omega_0 t)], \quad (3)$$

where $\omega_0 = 2\pi/24(\text{hour})$ is the frequency of the diurnal tide, t is the local time, Q_0 is the daily mean heating rate, and $m = 1, 2, 3, 4$ correspond to 24 h, 12 h, 8 h and 6 h tides, respectively. The harmonic fits at 50 and 90 km are given in Figure 1 with dashed lines. The harmonic fit roughly follows the diurnal variation of the heating rate but cannot reproduce the details, particularly around sunrise and sunset. More harmonics could be added to achieve a better fit but would have no impact on the amplitude or phase of the first four harmonic components. Figure 2 gives the vertical profiles of the harmonic components of the heating rate at the equator at equinox. There are several peaks in the daily mean heating rate. The lower one is near the stratopause, where the harmonic components are also large. There is a

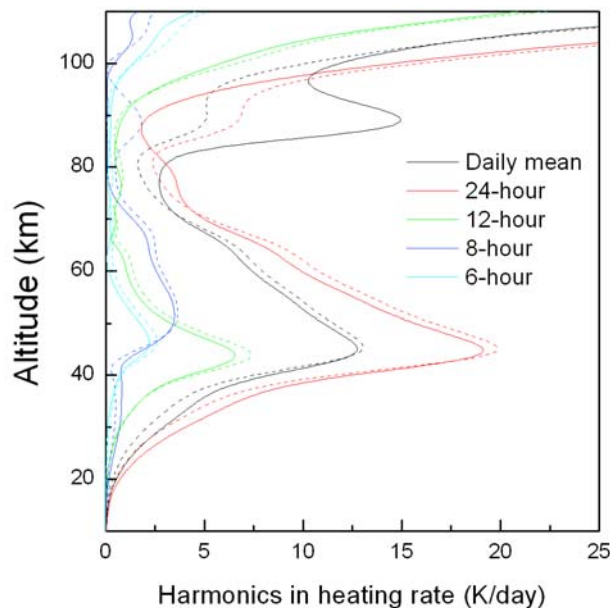


Figure 2. Vertical profiles of the amplitudes of harmonics in heating rate at the equator and the equinox. Solid line is photochemical model results. Dashed line is Strobel/Zhu's parameterization.

second peak at about 90 km, while all four of the harmonic components are very small there.

[15] The components of the heating from the Strobel/Zhu model using the model ozone profile are also given in Figure 2 (dashed lines). In the mesopause region, there are large discrepancies between the parameterization and the results of the 1-D model. Calculations for other latitudes and seasons (not shown) give similar results. The Strobel/Zhu model removes the energy that goes into photodissociation in the upper mesosphere [Zhu, 1994] but, because it does not include the heat from exothermic reactions, is not able to restore that energy to the net heating. Their parameterization therefore omits a process that is a major contribution to the heat source and, moreover, one that is stronger during night than during day. As a result, use of this parameterization alone both overestimates the magnitude of some components of tidal forcing (especially the 24 h and 8 h components) and underestimates the daily mean heating rate. However, above 100 km and below 70 km, where almost all of the absorbed solar energy immediately appears as heat in the atmosphere, the Strobel/Zhu model gives very good results. Strobel [1978] showed that the heating rate is mainly due to ozone heating below the mesopause while it is mainly due to the Schumann-Runge continuum (SRC) and the Schumann-Runge bands (SRB) of O_2 above 100 km.

[16] We are not able to use the available observations to determine the harmonic components of the heating rate in the upper mesosphere: the Strobel/Zhu heating rate model does not include all the information needed and there are not sufficient observations of the trace species that contribute to the exothermic reactions to calculate the chemical heating directly. We also cannot determine the heating rate in the thermosphere because we do not have global observations of the O_2 distribution. Therefore, we use Aura/MLS observed ozone data and the Strobel/Zhu parameterization

of ozone heating to characterize the features of the ozone heating rate between 10 and 70 km.

3. Calculation of the Diurnal Variation in Heating Rate and Its Hough Modes Using Satellite Observations of Ozone

3.1. Data Set and the Method of Calculating the Harmonic Components of the Heating Rate

[17] The NASA Earth Observing System (EOS) Aura satellite, launched on 15 July 2004, is in a Sun-synchronous near-polar 705 km altitude orbit. It gives daily global coverage with about 14 orbits per day. MLS (Microwave Limb Sounder) is one of the instruments aboard the Aura satellite. MLS has been making atmospheric science observations since 13 August 2004. MLS measures ozone, temperature and other chemical species from 215 to 0.02 hPa, about 10 to 75 km, with a vertical resolution of about 3 km. The Aura/MLS orbital plane has a high inclination angle and the scans are within the orbital plane, which results in equal numbers of scans up to 82° in both hemispheres. Daily MLS data can be used to construct two global maps of ozone and temperature vertical profiles, near noon and midnight. We use level 2, version 2.2 of MLS daytime ozone and temperature data for our analysis.

[18] The validation studies of the MLS v2.2 ozone data show that the systematic uncertainty from 68 hPa to 0.2 hPa (from about 18 km to 60 km) is better than 8%, the systematic bias at 215 hPa is about 10–20%, and the systematic bias above 65 km (~ 0.01 hPa) is larger than 20% [see Froidevaux *et al.*, 2008, Table 2]. From Strobel [1978], we can see that the ozone heating rate is directly proportional to the ozone density and also depends on the ozone column density along a slant path to the top of the atmosphere. Even a significant systematic bias in the ozone above 65 km will have little impact on the column density because of the very low ozone density above there. Therefore, the accuracy of the heating rate is mainly dominated by the accuracy of ozone density in the vertical range 18–60 km. The accuracy of the ozone heating rate is about equal to the accuracy of the MLS observed ozone density, i.e., less than 8% uncertainty.

[19] The ozone heating rate analysis is in four steps.

[20] 1. Each ozone vertical profile is interpolated to a uniform vertical grid with 1 km spacing from 10 km to 70 km.

[21] 2. The daily averaged ozone profile for day and that for night are calculated at each latitude bin (i.e., averaging in longitude). This step conserves the ozone distribution that contributes to the migrating tide and removes any potential nonmigrating tidal signals. The ozone profiles are sorted into overlapping latitude bins that are 10 degrees wide with centers offset by 5° , extending from $80^\circ S$ to $80^\circ N$. The times of daily observations are centered at two local times, near midday and midnight, corresponding to the ascending and descending phases respectively.

[22] 3. The diurnal variation of the vertical profile of the ozone heating rate in each latitude bin is calculated using the MLS observed daytime ozone distribution and the parameterization of Strobel/Zhu, along with the diurnal variation of solar zenith angle for the specific latitude and day of year. The calculation uses the MLS observed midday ozone concentration to represent all daytime hours: a good

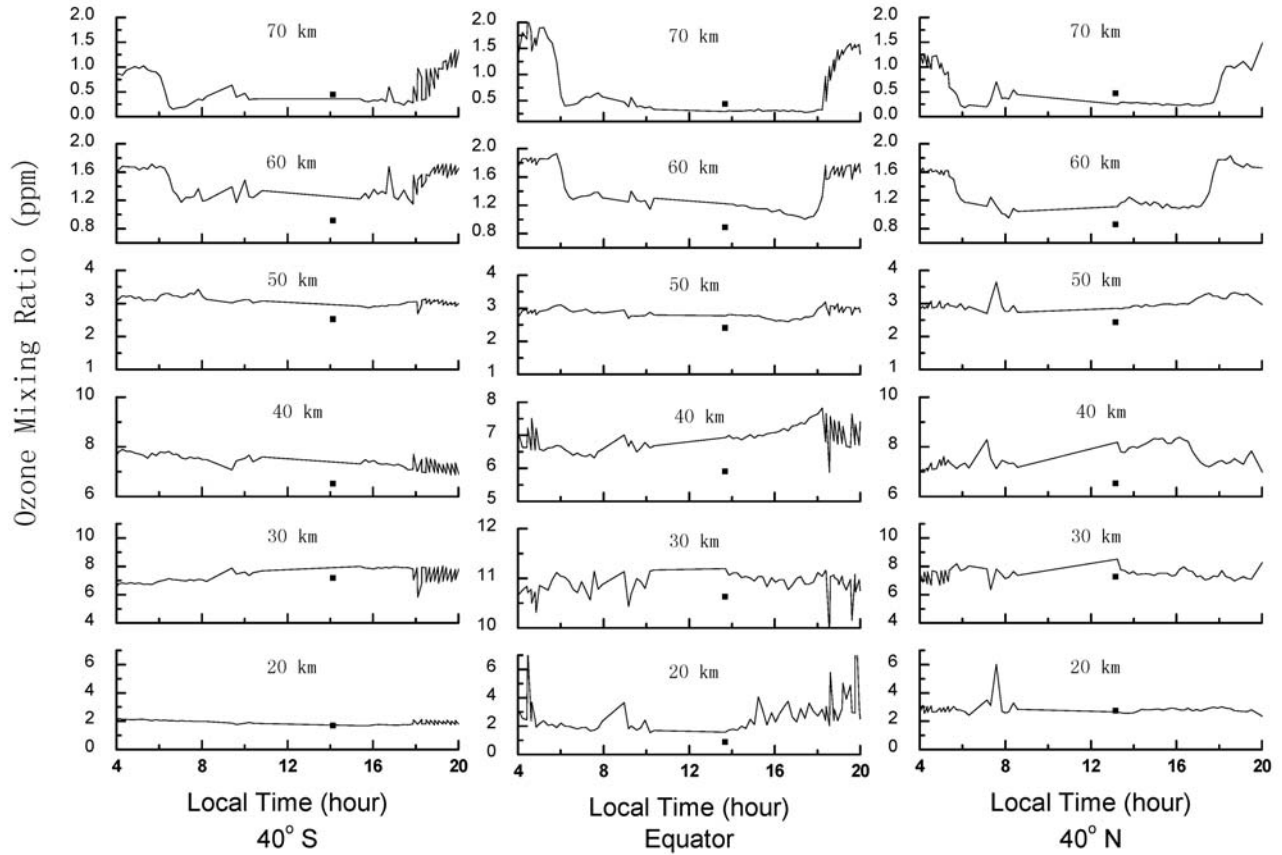


Figure 3. The diurnal variation of ozone mixing ratio observed by TIMED/SABER and Aura/MLS for day 80 in 2005. Solid line is the diurnal variations of the ozone mixing ratio which are pieced together using a 70 day window of TIMED/SABER ozone observation at 6 altitudes. Squares are the Aura ozone observations.

approximation because the ozone mixing ratio in this altitude range is almost constant during the daytime. To verify this, Figure 3 shows the diurnal variation of ozone mixing ratio observed by TIMED/SABER. The diurnal variations of ozone from TIMED/SABER are pieced together using a 70 day window centered at day 80 in 2005. The MLS daytime ozone averaged over the same period is also shown. Figure 3 shows that, below 50 km, there is no obvious diurnal variation, as expected due to the long chemical lifetime. Above 60 km, there is a marked day-night variation in ozone. However, during the daytime, from 0600 to 1800, the ozone mixing ratio variations are small. Therefore, it is a good approximation to use midday ozone data observed by MLS to represent daytime ozone profiles at all times during the portion of the day that the atmosphere is in daylight. Also, note from Figure 3 that the SABER ozone mixing ratio is larger than that from MLS, which is consistent with the comparisons shown by Rong *et al.* [2009, Figure 13]. The possible reasons for the differences may be the negative biases in SABER temperature and the error in retrieved pressure [Rong *et al.*, 2009]. Validation studies of the MLS v2.2 ozone data show that they also have systematic uncertainty of 5–20% from 68 hPa to 0.01 hPa (about 18 km to 65 km) [Froidevaux *et al.*, 2008]. Only the daytime ozone is used for the heating rate calculation because the nighttime heating is zero. We divide each day into 60 local time points with a step of 24/60 h. The global distribution of the heating rate for each local time point

is calculated, taking account of the solar zenith angle dependence on latitude, time of year, and local time. In this step, the calculation also considers the annual variation of the Sun–Earth distance; the energy input to the earth from the sun varies annually by 6.6%, with the maximum value in January and the minimum value occurring in July. Solar variability due to the 11 year cycle or shorter term variations is not included.

[23] 4. The global distributions of the daily mean heating rate and the 24 h, 12 h, 8 h, and 6 h components are separated using least squares fitting. The method used to separate the daily mean and the harmonic components of heating rate is the same as in the temperature analysis of Xu *et al.* [2007, equation (6)].

[24] After the 4 steps, we have a data set of each component of the heating rate for each latitude, altitude, and day from August 2004 to December 2008.

3.2. Calculation of the Diurnal Hough Components of the Ozone Heating Rate

[25] The diurnal component of the ozone heating rate (the $m = 1$ term in equation (3)) at each latitude, altitude and day can be represented by two terms, Q_1^c and Q_1^s .

$$q_1(d, \theta, z, t) = Q_1^c(d, \theta, z) \cos(\omega_0 t) + Q_1^s(d, \theta, z) \sin(\omega_0 t). \quad (4)$$

Hough functions are eigenfunctions of Laplace's tidal equation. They are widely used in the analysis and theory of tides. The Hough mode represented as $\Theta_{s,n}(\theta)$, or (s, n) for

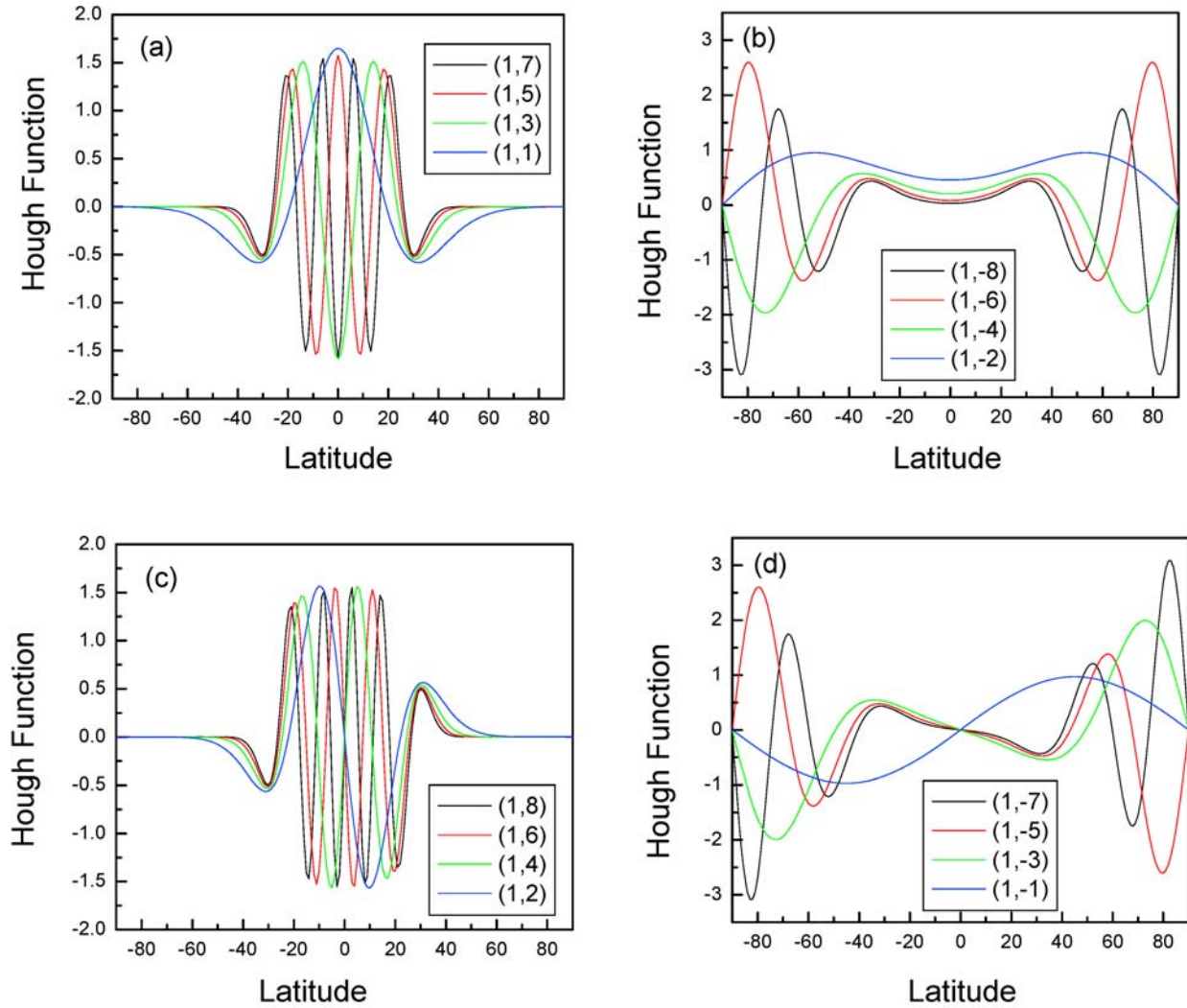


Figure 4. Hough functions for diurnal modes normalized to a maximum value of unity. (a and c) Propagating modes and (b and d) trapped modes. Figures 4a and 4b are symmetric modes, and Figures 4c and 4d are antisymmetric modes.

short, indicates a global wave form with zonal wave number s and index n , where n is positive for gravitational modes and negative for rotational modes. For the migrating diurnal tides, the symmetric and antisymmetric gravitational modes (or propagating modes) are $(1, 1)$, $(1, 3)$, ..., and $(1, 2)$, $(1, 4)$, The symmetric and antisymmetric diurnal rotational modes (or trapped modes) are designated by $(1, -2)$, $(1, -4)$, ..., and $(1, -1)$, $(1, -3)$, ... [e.g., *Forbes and Garrett, 1979*]. In particular, since some of the modes propagate vertically and others do not [e.g., *Chapman and Lindzen, 1970*], it is useful to know how the heating projects onto the propagating and nonpropagating modes. The Hough functions for the diurnal frequency form a complete orthogonal set and extend from 90°S to 90°N . The Hough functions used for expanding the heating are normalized such that the square of their area is one. The normalized functions satisfy the relation

$$\int_{-90^\circ}^{90^\circ} \Theta_{1,n}(\theta) \cdot \Theta_{1,m}(\theta) \cos(\theta) d\theta = \begin{cases} 1, & n = m \\ 0, & n \neq m \end{cases}, \quad n, m = \pm 1, \pm 2, \dots$$

Figure 4 shows 16 normalized Hough functions for the diurnal tide. Figures 4a and 4c correspond to propagating modes; Figures 4b and 4d correspond to trapped or evanescent modes. Figures 4a and 4b are symmetric modes; Figures 4c and 4d are antisymmetric modes [*Forbes, 1995*].

[26] The ozone heating rate calculated from the Aura/MLS ozone data can be obtained in the latitude range from 80°S to 80°N . To fit the heating to Hough functions, we must extend the heating rate to the poles. Generally speaking, the heating rate at subharmonics of a solar day (i.e., periods of 24, 12, 8 and 6 h) should be zero at the South and North Pole. The heating rates between 80°S and 90°S and between 80°N and 90°N are calculated by interpolation.

[27] Since we are considering only the diurnal component of the heating rate, we can fully express this local time dependent quantity by a pair of scalar values, the sine and cosine coefficients. These two diurnal components of the

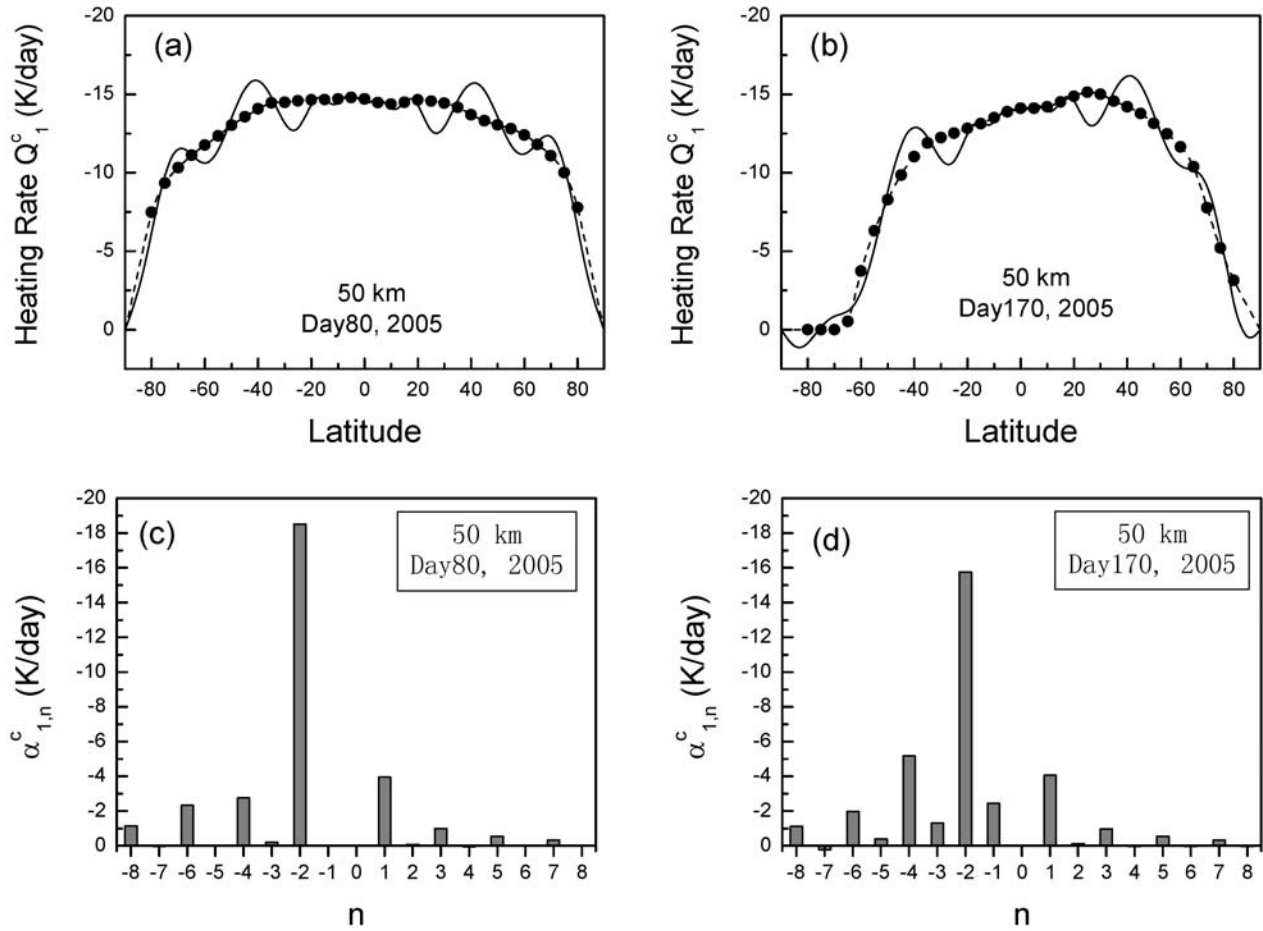


Figure 5. Latitude distribution of the diurnal component of ozone heating at 50 km at (a and c) day 80 (21 March) and (b and d) day 170 (19 June) in 2005. In Figures 5a and 5b, dots are heating rates calculated from MLS ozone; dashed line is extension of the calculated heating rates to the south and north poles; and solid line is fitting by diurnal Hough functions. Figures 5c and 5d show the magnitudes of the diurnal heating Hough modes $(1,n)$, where n varies from -8 to 8 .

global heating rate are expanded in terms of normalized Hough functions $\Theta_{1,n}(\theta)$,

$$Q_1^c(d, \theta, z) = \sum_{n \neq 0} \alpha_{1,n}^c(d, z) \Theta_{1,n}(\theta), \quad (5a)$$

$$\alpha_{1,n}^c(d, z) = \int_{-90^\circ}^{90^\circ} Q_1^c(d, \theta, z) \Theta_{1,n}(\theta) \cos(\theta) d\theta, \quad (5b)$$

$$Q_1^s(d, \theta, z) = \sum_{n \neq 0} \alpha_{1,n}^s(d, z) \Theta_{1,n}(\theta), \quad (5c)$$

$$\alpha_{1,n}^s(d, z) = \int_{-90^\circ}^{90^\circ} Q_1^s(d, \theta, z) \Theta_{1,n}(\theta) \sin(\theta) d\theta. \quad (5d)$$

Here $\alpha_{1,n}^c(d, z)$ and $\alpha_{1,n}^s(d, z)$ are the coefficients of the cosine and sine terms in the n th component of the Hough modes. Figure 5 gives examples of the latitudinal distribution of the cosine term $Q_1^c(\theta, z)$ in the diurnal component of the heating rates and its Hough mode fit at 50 km for day 80 and day 170 in 2005. The coefficients of the cosine term in

the n th component of the Hough modes are also given. Figure 5 shows that the fitting using the 16 Hough modes shown in Figure 4 can reconstruct the outline of the latitudinal distribution of the diurnal component in the heating rate but differs in the details. The sum using this finite set of Hough modes has latitudinal variability not seen in the heating itself. From Figure 5 we can see that the smoothness of the heating does not project well onto any Hough modes except the first few, which also have little structure in latitude (a detailed discussion is given in section 4).

[28] Using equations (5a)–(5d), the diurnal heating rate equation (4) can be expressed as the combination of Hough functions

$$q_1(d, \theta, z, t) = \sum_{n \neq 0} \left[\alpha_{1,n}^c(d, z) \cos(\omega_0 t) + \alpha_{1,n}^s(d, z) \sin(\omega_0 t) \right] \Theta_{1,n}(\theta). \quad (6)$$

4. Seasonal Variations in Diurnal Hough Components of the Heating Rate

[29] The seasonal and interannual variations of the atmospheric diurnal tide, which include semiannual (SAO),

annual (AO), and quasi-biennial (QBO) oscillations, have received considerable attention in recent years, but have not been successfully explained [e.g., *Xu et al.*, 2009]. Mechanisms that have been proposed include variations in tidal propagation due to modulation of the background zonal wind in the middle atmosphere and the effects of a seasonal cycle in the momentum deposition from small-scale gravity waves [e.g., *Hagan et al.*, 1995, 1999; *McLandress*, 2002a, 2002b; *Mayr and Mengel*, 2005]. It is also possible that the tidal forcing by ozone heating plays a role. Here we determine variations in the heating that could be applied to an investigation of its role.

4.1. Seasonal Variations of the Total Diurnal Component of Heating Rate

[30] From equation (4), the amplitude of the diurnal component in the heating rate can be calculated by

$$Q_1(d, \theta, z) = \sqrt{[Q_1^c(d, \theta, z)]^2 + [Q_1^s(d, \theta, z)]^2}. \quad (7)$$

Figure 6 gives the latitudinal distributions of the amplitude of the diurnal component in the ozone heating rate Q_1 over the period from August 2004 to December 2008 at altitudes of 55, 45, 35, and 25 km. From Figure 6 we can see that in the middle and high latitudes, the annual oscillation (AO) dominates the seasonal variation. There also is semiannual oscillation (SAO) signature in high latitudes. The maximum amplitude of the diurnal component in the heating rate occurs during the December/January solstice period and is displaced toward the south hemisphere. This is because of the annual variation of the Sun-Earth distance, which contributes a 6.6% annual variation of solar energy input to the atmosphere. In the upper levels (45 and 55 km), where the ozone heating is largest, there is no obvious QBO in the diurnal component in the heating rate. At 25 km, the QBO signature is apparent in low latitudes as heating maxima in 2006 and 2008. The heating variations are a direct result of the significant variations in lower stratospheric ozone with the QBO [*Baldwin et al.*, 2001]. We also analyzed the daytime ozone observed by Aura/MLS, and found a similar QBO signal (not shown). However, the heating is very weak at 25 km: an order of magnitude less than that at 45 km.

[31] The contributions of the periodic variations in the diurnal component in the ozone heating rate to the net variability can be quantified. We express the long-term variations of the amplitude of the diurnal heating from August 2004 to December 2008 as the sum of the SAO, AO, and QBO variations and a linear trend.

$$\begin{aligned} Q_1 = & \bar{Q}_1 + \mu_Q(d - d_c) + Q_{1,SAO} \cos\left[\frac{2\pi}{182.5(\text{day})}(d - d_{Q,SAO})\right] \\ & + Q_{1,AO} \cos\left[\frac{2\pi}{365(\text{day})}(d - d_{Q,AO})\right] \\ & + Q_{1,QBO} \cos\left[\frac{2\pi}{P_{Q,QBO}(\text{day})}(d - d_{Q,QBO})\right], \end{aligned} \quad (8)$$

where \bar{Q}_1 is the average value of Q_1 during August 2004 to December 2008; μ_Q is the trend in Q_1 over this period; d_c is the central day of the 4 year observation period; $Q_{1,SAO}$, $Q_{1,AO}$, and $Q_{1,QBO}$ are the amplitudes of the SAO, AO and

QBO in Q_1 over the 4 years; and $d_{Q,SAO}$, $d_{Q,AO}$, and $d_{Q,QBO}$ are the phases of the three oscillations. Generally speaking, the period of the QBO in lower stratospheric winds in the equatorial region is variable within the range 18–34 months. Therefore, the period of the QBO is also a variable, $P_{Q,QBO}$. The trend and the SAO, AO and QBO in the diurnal heating rate are determined simultaneously using a nonlinear least squares fitting method. The method used to quantify the seasonal and longer-term variability of the diurnal component of ozone heating rate is similar to that used in the temperature analysis by *Xu et al.* [2007, 2009]; see those papers for more detailed discussion.

[32] Figure 7 gives the averaged values and the amplitudes and phases of the seasonal oscillations of the diurnal component in the heating rate as a function of latitude and altitude. The maximum of the averaged heating rate is about 16 K/d near the altitude of 47 km at the equator. The peak SAO amplitude of 3.4 K/d occurs in high latitudes near 52 km (see Figure 7b), and the phase is near the equinox (Figure 7e). This is because, poleward of the Arctic or Antarctic Circles, the diurnal periodicity of heating disappears completely near winter solstice, when there is no heating. The diurnal variability is also small near summer solstice, when the heating is spread over 24 h. As a result, there are maxima in the diurnal variability of the heating at the equinoxes. This can also be seen in the relative minima in the diurnal heating near the summer poles in Figure 6.

[33] The AO in high latitudes (see Figure 7c) also reflects this heating variation. Figure 7f shows that the annual oscillation reaches maximum near the summer solstice. The maximum amplitude of the AO is about 5.7 K/d near 47 km. Figure 7d shows that the QBO in the diurnal component of the heating rate is very weak, about 0.2 K/d near the equator, which is only 1–2% of the averaged heating rate near the equator in the upper stratosphere and lower mesosphere. In the lower stratosphere, there is an obvious QBO in the heating rate (also see Figure 6). For instance, at 25 km, the amplitude of the QBO in the diurnal component of the heating rate at the equator is 0.13 K/d, while the averaged heating rate is 1.3 K/d. At this altitude, the amplitude of the QBO in the heating rate is 10% of the averaged heating rate near the equator. Even though there are significant variations in the diurnal component of ozone heating rate and ozone density with the QBO [*Baldwin et al.*, 2001], these are larger in the lower stratosphere whereas the diurnal heating peaks substantially above there. There are large variations in the calculated period and phase of the QBO in diurnal heating (not shown). It is likely that the duration of the data record is too short (only 53 months), and the amplitude of QBO in the diurnal heating rate is too weak, to determine period and phase reliably.

[34] The trend in the heating is not reliable in these calculations because of the neglect of the solar cycle variations in solar flux, and is also not shown.

4.2. Seasonal Variations of the Diurnal Hough Modes in the Heating Rate

[35] Using this method, we can also calculate the seasonal variations in each Hough mode of the diurnal component of heating rate. We determine the SAO, AO, QBO and linear trend from August 2004 to December 2008 of $\alpha_{1,n}^c(z)$ and $\alpha_{1,n}^s(z)$ of each Hough component in equation (6) using a similar method to that presented in equation (8).

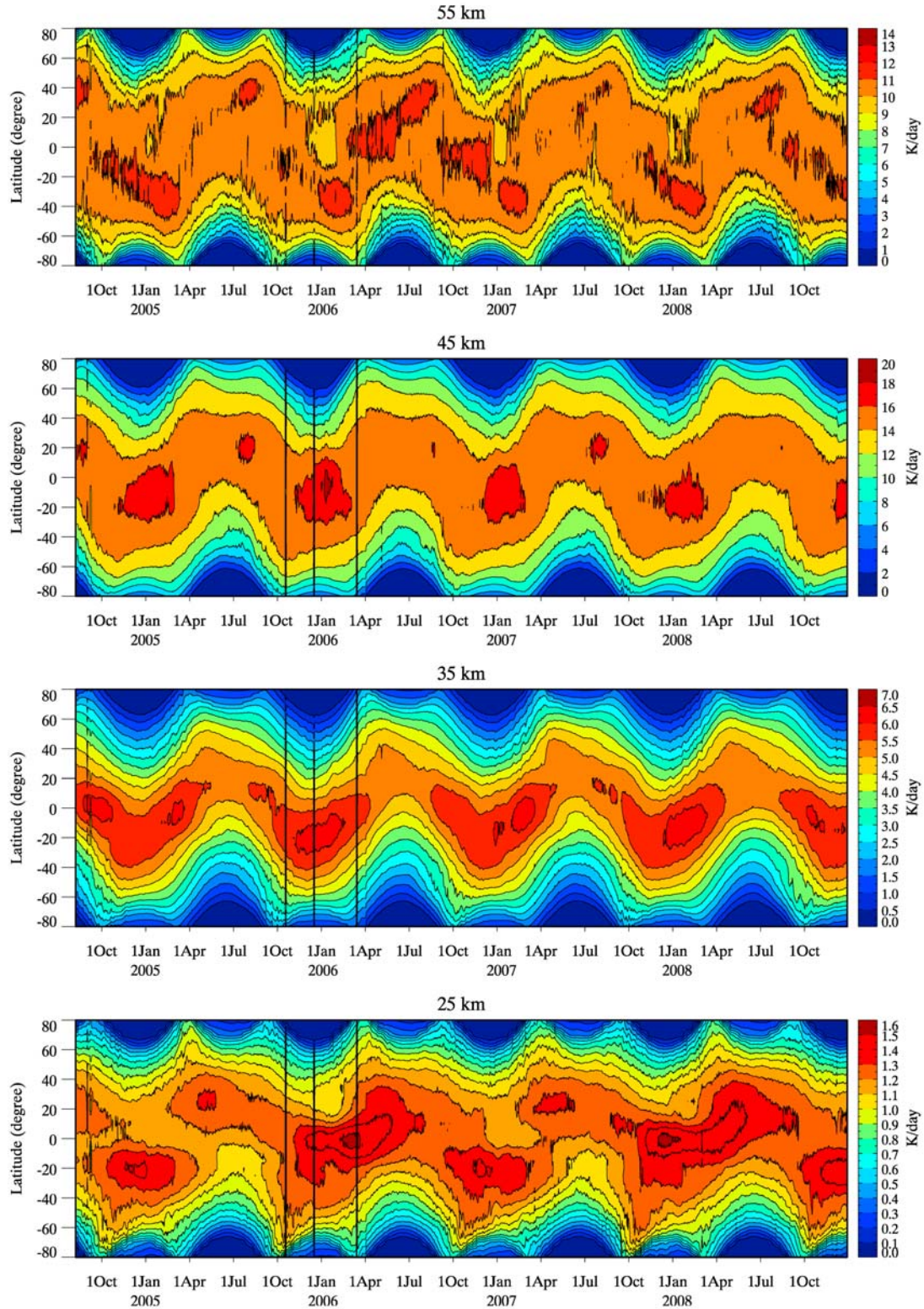


Figure 6. Latitude-time sections of the diurnal component of the ozone heating rate over the period from August 2004 to December 2008 at four altitudes.

[36] The magnitude of the cosine component of the heating $|Q_1^c(d, \theta, z)|$ is much larger than that of the sine component $|Q_1^s(d, \theta, z)|$ because the phase (at which the heating rate reaches maximum) of the diurnal component of

heating rate is around 12:00LT. As a result, the cosine terms in equation (6) are much larger than the sine terms, $|\alpha_{1,n}^c(d, z)| \gg |\alpha_{1,n}^s(d, z)|$. In this section, we mainly

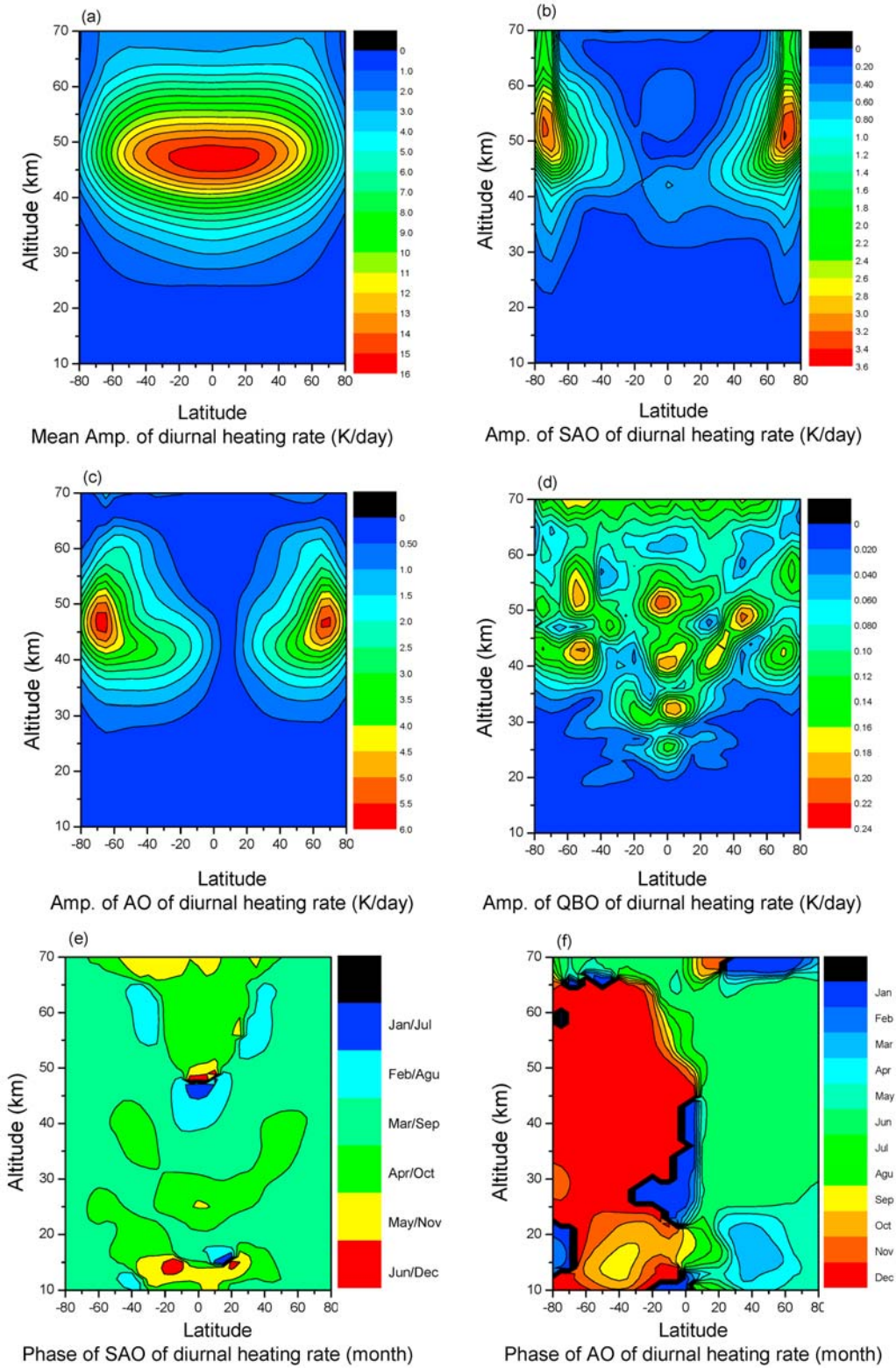


Figure 7. (a) The mean ozone heating rate over the period from August 2004 to December 2008 (53 months total); the amplitudes of the (b) SAO, (c) AO, and (d) QBO; and phases of the (e) SAO and (f) AO variations in the heating rate. The phase labels give the month of maximum heating.

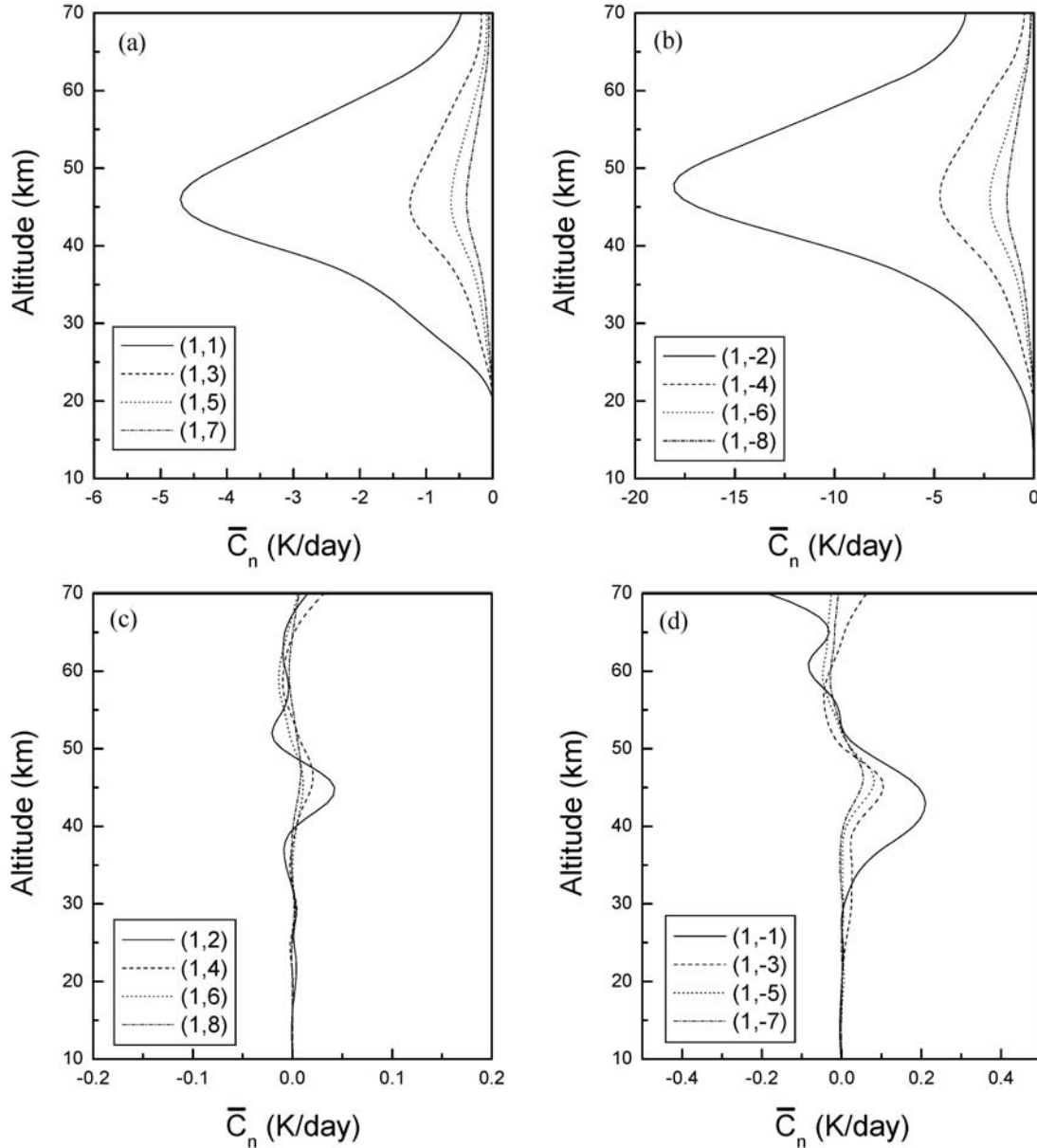


Figure 8. Hough mode decomposition of the cosine component of the 4 year average diurnal component of the ozone heating. Negative values indicate that the heating maximum occurs at or near midday.

discuss the characteristics of the Hough functions of the cosine component of the heating.

4.2.1. Mean Diurnal Hough Components of Heating Rate

[37] Figure 8 gives the coefficients of the Hough modes of the 4 year mean diurnal component of ozone heating rate \bar{C}_n . The coefficients in Figures 8a and 8b are negative because the heating rate reaches maximum near the cosine function minimum at noon (1200 LT). Figure 8 shows that (1,1) is the largest heating source in the propagating modes; it has a peak of about -4.7 K/d near 46 km. The (1,3) mode is the second largest propagating source with a peak value of about -1.2 K/d. In the trapped modes, the (1,-2) mode is the strongest mode with a peak of about -18 K/d near 48 km, about four times larger than the (1,1) mode. The (1,-4) mode is the second strongest trapped mode; it reaches about

-4.7 K/d near 47 km and has a similar magnitude to the (1,1) mode. These results are approximately consistent with the results of Groves [1982]. Figures 8c and 8d shows that the antisymmetric modes of the 4 year mean diurnal components of ozone heating are much weaker than the symmetric modes.

4.2.2. Semiannual Variations in the Diurnal Hough Components of Heating Rate

[38] Vertical profiles of the SAO in the symmetric Hough modes are given in Figure 9. Propagating modes are shown in Figures 9a and 9b; trapped modes are in Figures 9c and 9d. The SAO in the antisymmetric modes is very small and is not shown. The peak amplitude of the SAO in (1,1) is 0.45 K/d, which is about 10% of its mean value shown in Figure 8. Figure 9b shows that the SAO phases vary strongly but smoothly from near solstice at the upper level

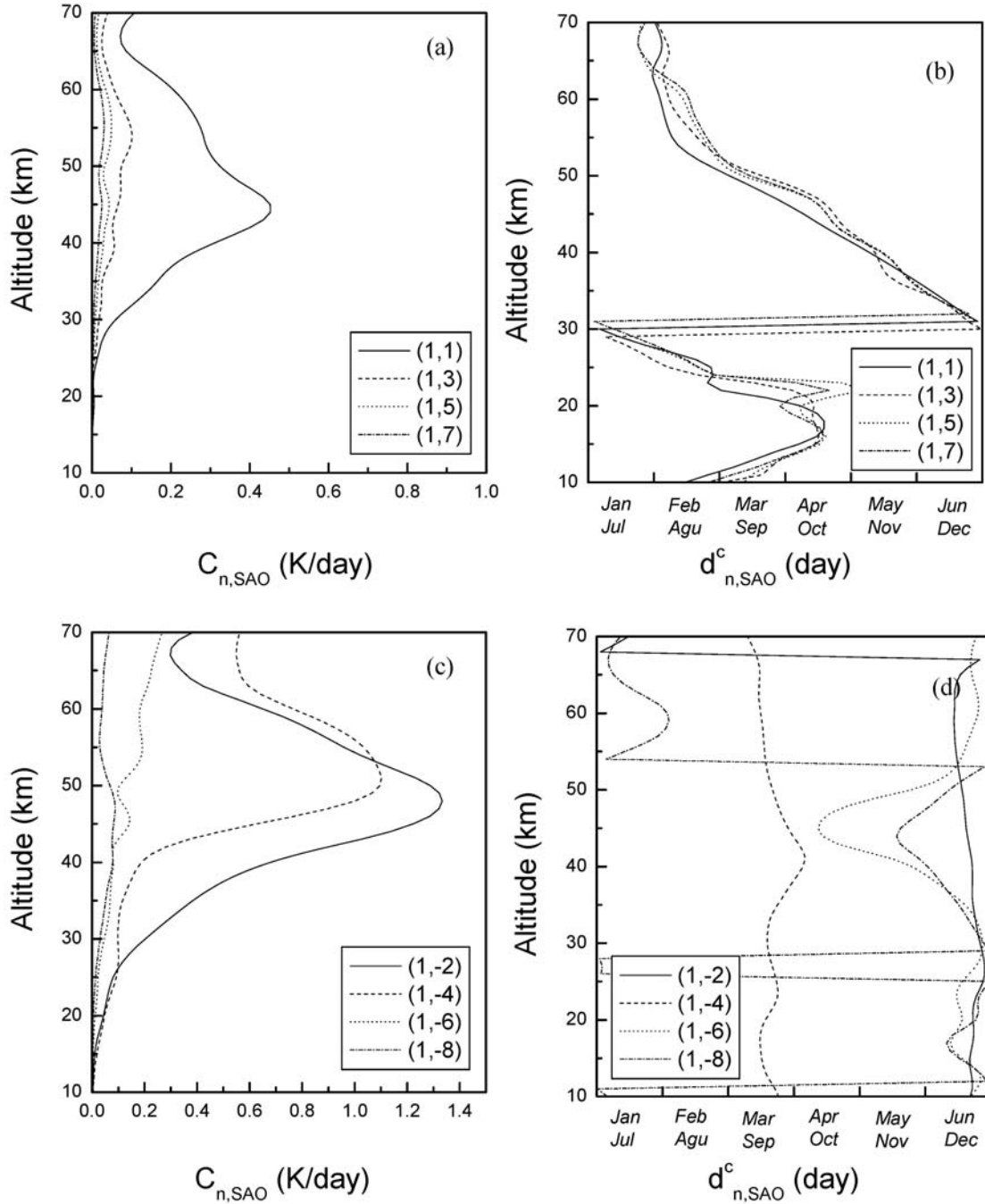


Figure 9. (a and c) Amplitudes and (b and d) phases of the SAO variation in the Hough modes of the cosine coefficient of the diurnal heating. The phase labels give the month of the maximum heating which, for the symmetric modes, is the month of minimum of the (negative) Hough mode (see Figure 8).

(70 km), through equinox in the upper stratosphere to again near-solstice around 30 km. Near the altitude of the SAO peak (around 46 km), the phase is near the equinox. Because the average values are negative (see Figure 8a), this means that the heating rate reaches minimum near the equinoxes.

[39] Figure 9c shows that the peak amplitude of the SAO in (1,-2) is 1.3 K/d near 50 km, which is about 7% of its mean value; its phase is around solstice. The trapped Hough mode, (1,-4) has a peak near 50 km and an amplitude rel-

ative to its mean value of 25%. The amplitudes of the other modes are very weak. Figure 9d shows that the phase of the (1,-2) mode is near the solstice, and the phase of (1,-4) mode is near the equinox.

4.2.3. Annual Variations in the Diurnal Hough Components of Heating Rate

[40] Vertical profiles of the AO in the symmetric and asymmetric Hough modes are given in Figures 10 and 11, respectively. The peak magnitudes in the symmetric Hough

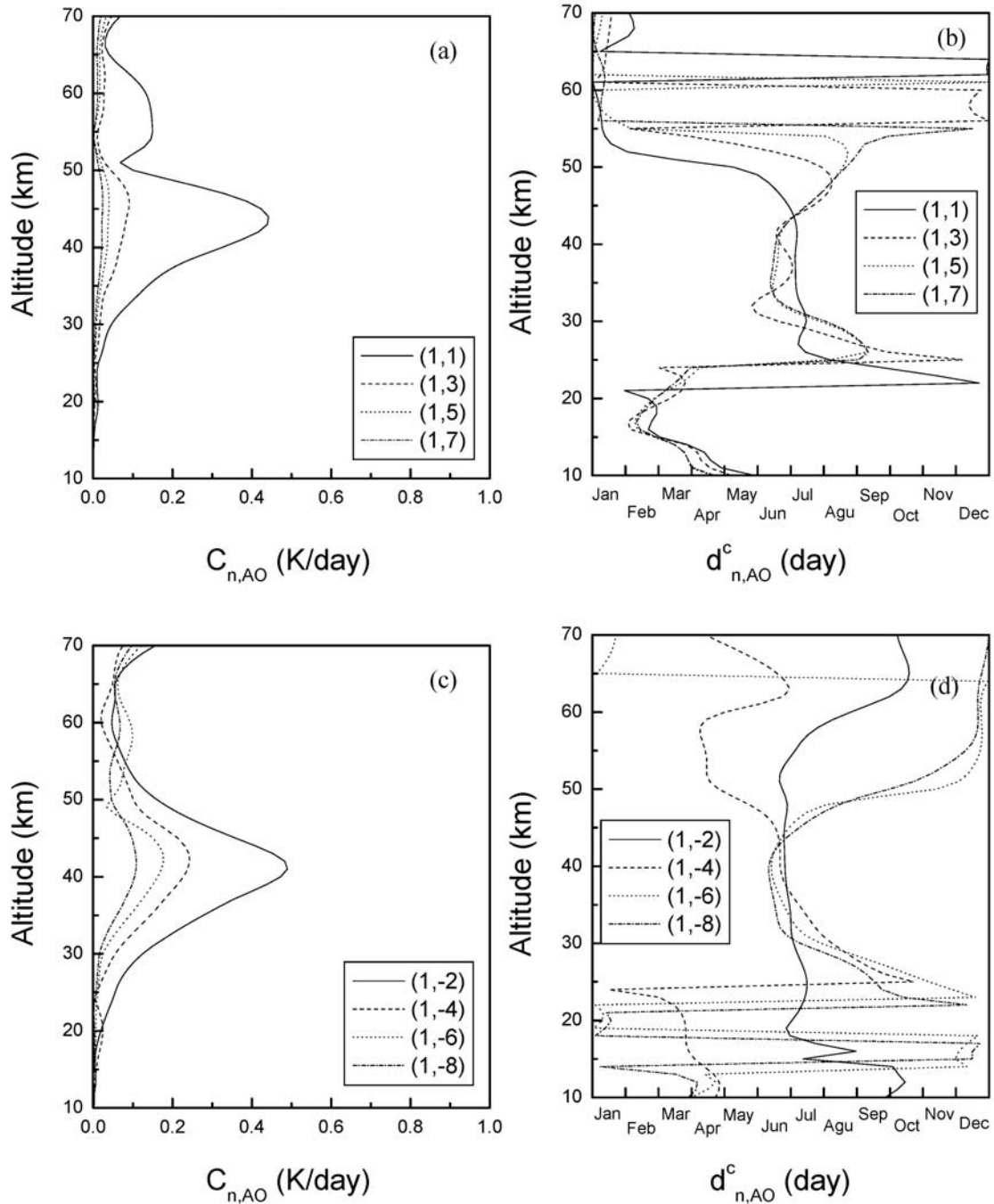


Figure 10. (a and c) Amplitudes and (b and d) phases of the AO variation in the symmetric Hough modes of the cosine coefficient of the diurnal heating. The phase labels give the month of the maximum heating which, for the symmetric modes, is the month of minimum of the (negative) Hough mode (see Figure 8).

modes are about 0.5 K/d and the phases near the altitudes of their amplitude peaks give maximum heating around the December/January solstice. The diurnal heating rates in these modes are larger in the December/January solstice period than the June/July solstice because of the annual variation of the Sun-Earth distance, which contributes a 6.6% annual variation of solar energy input to the atmosphere.

[41] The annual variations in the propagating antisymmetric Hough modes are less than 0.2 K/d (Figure 11a),

which make these modes the weakest of the Hough mode components in terms of annual variations. The strongest annual variation of these is seen in the (1,-1) antisymmetric Hough mode, which reaches 3.6 K/d near 45 km (Figure 11c). However, the 4 year mean value of this mode is only 0.2 K/d (see Figure 8d). The phase of the AO in this mode is around the December/January solstice. From Figure 4d, we can see that this means that near the December/January solstice, the magnitude of the diurnal component in heating rate is

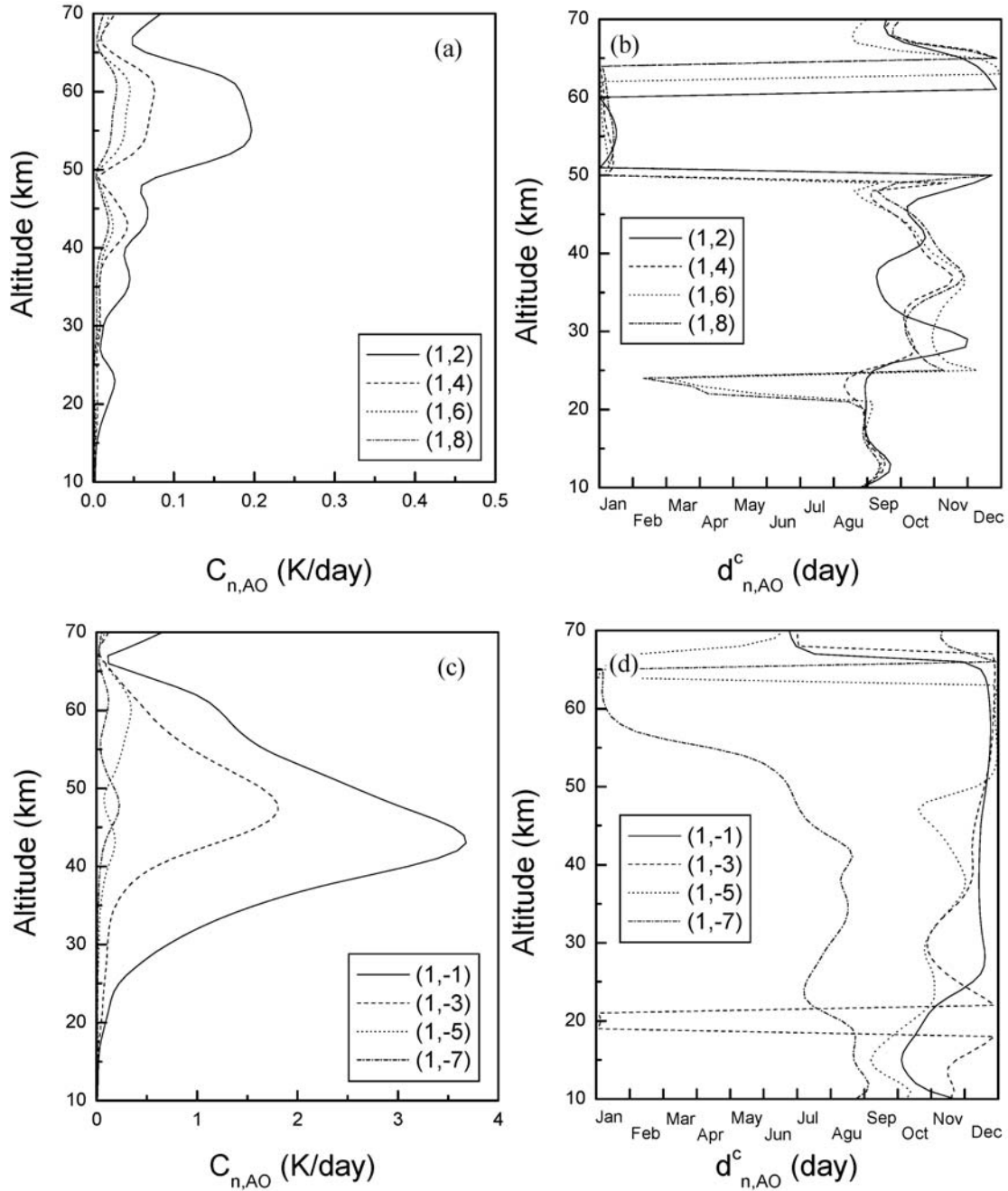


Figure 11. (left) Amplitudes and (right) phases of the AO variation in the antisymmetric Hough modes of the cosine coefficient of the diurnal heating. The phase labels give the month of the maximum of the (positive) Hough modes (see Figure 8).

stronger in the southern than in the northern hemisphere, while the opposite is true near the June/July solstice.

4.2.4. Quasi-biennial Oscillation Signatures in the Diurnal Hough Components of Heating Rate

[42] The QBO amplitude of every Hough mode is very weak. The strongest QBO signals are found in the (1,1) and (1,-2) modes but their amplitudes are only about 0.1–0.2 K/d. In an analysis of the variations in the global structure of temperature, *Xu et al.* [2007] found that the QBO analysis was quite sensitive to the length of the data period used. The Aura observations cover only two cycles of the QBO so the

determination of the amplitude, phase and period is subject to significant uncertainty. Therefore, for the presently available short period of Aura/MLS observations, we do not want to say more than that the QBO signature in the diurnal component of ozone heating is weak. The amplitude and phase of the QBO are included in the fits, as described by equation (8) and, for completeness, the QBO parameters are given in the auxiliary material data sets.¹

¹Auxiliary materials are available at <ftp://ftp.agu.org/apend/jd/2009jd013179>.

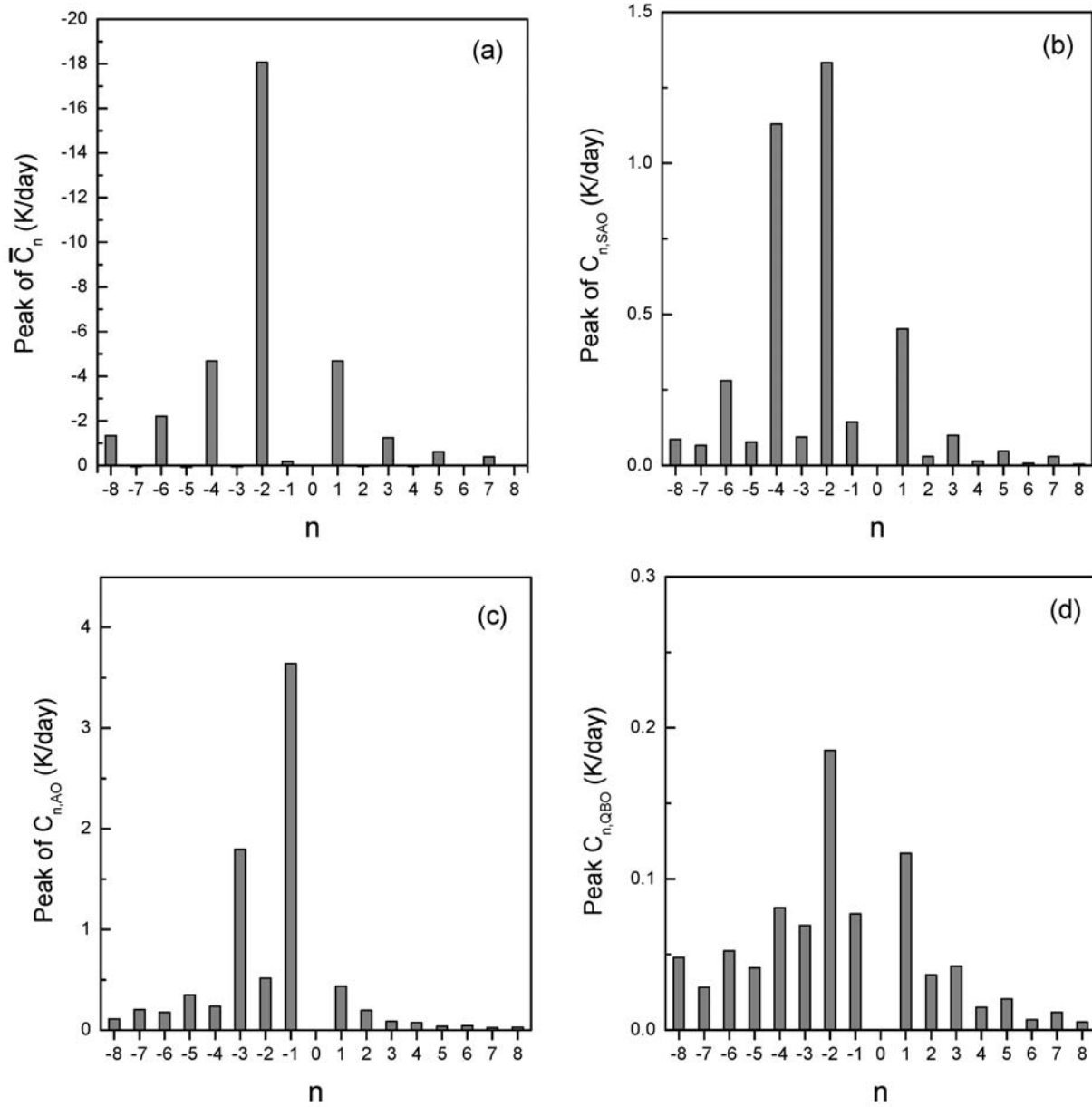


Figure 12. The magnitudes of the mean and periodic variations of the diurnal heating Hough modes $(1, n)$, where n varies from -8 to 8 . (a) The mean over the data record, (b) SAO, (c) AO, and (d) QBO.

4.2.5. Summary of the Seasonal Variations of the Diurnal Hough Modes in the Heating Rate

[43] Figure 12 compares the peak magnitudes of each Hough mode of the diurnal component of the ozone heating rate, as discussed in sections 4.2.1–4.2.4. The modes with $n > 0$ are propagating and those with $n < 0$ are trapped. Figure 12 shows that the diurnal component of the ozone heating projects most strongly onto the trapped modes. The strongest seasonal oscillations also take place in the trapped modes. The $(1, 1)$ mode is the strongest propagating mode with a magnitude of 4.7 K/d. The strongest trapped mode is $(1, -2)$ with a magnitude of 18 K/d, about 4 times larger. Results of Groves [1982] show that the $(1, 1)$ mode has a magnitude of about 50 mW/kg (~ 4.32 K/d) and the $(1, -2)$

mode has a magnitude of about 200 mW/kg (~ 17.28 K/d), likewise a factor of 4 difference. Figure 12 also shows that the strongest propagating mode, $(1, 1)$, is comparable to the $(1, -4)$ trapped mode. The $(1, -1)$ and $(1, -3)$ modes are the strongest antisymmetric trapped modes. They describe the annual variation of the ozone heating rate; their annual average values are very small.

[44] We take the strongest propagating mode $(1, 1)$ and the strongest trapped mode $(1, -2)$ as examples to illustrate the seasonal variation of the heating rate. Figure 13 gives the seasonal and vertical variations of the amplitudes of these two Hough modes of the cosine of the diurnal heating (i.e., the $\alpha_{1,1}^c(d, z)$ and $\alpha_{1,-2}^c(d, z)$ terms) from 2004 to 2008 calculated from equations (5a)–(5d). The propagating $(1, 1)$

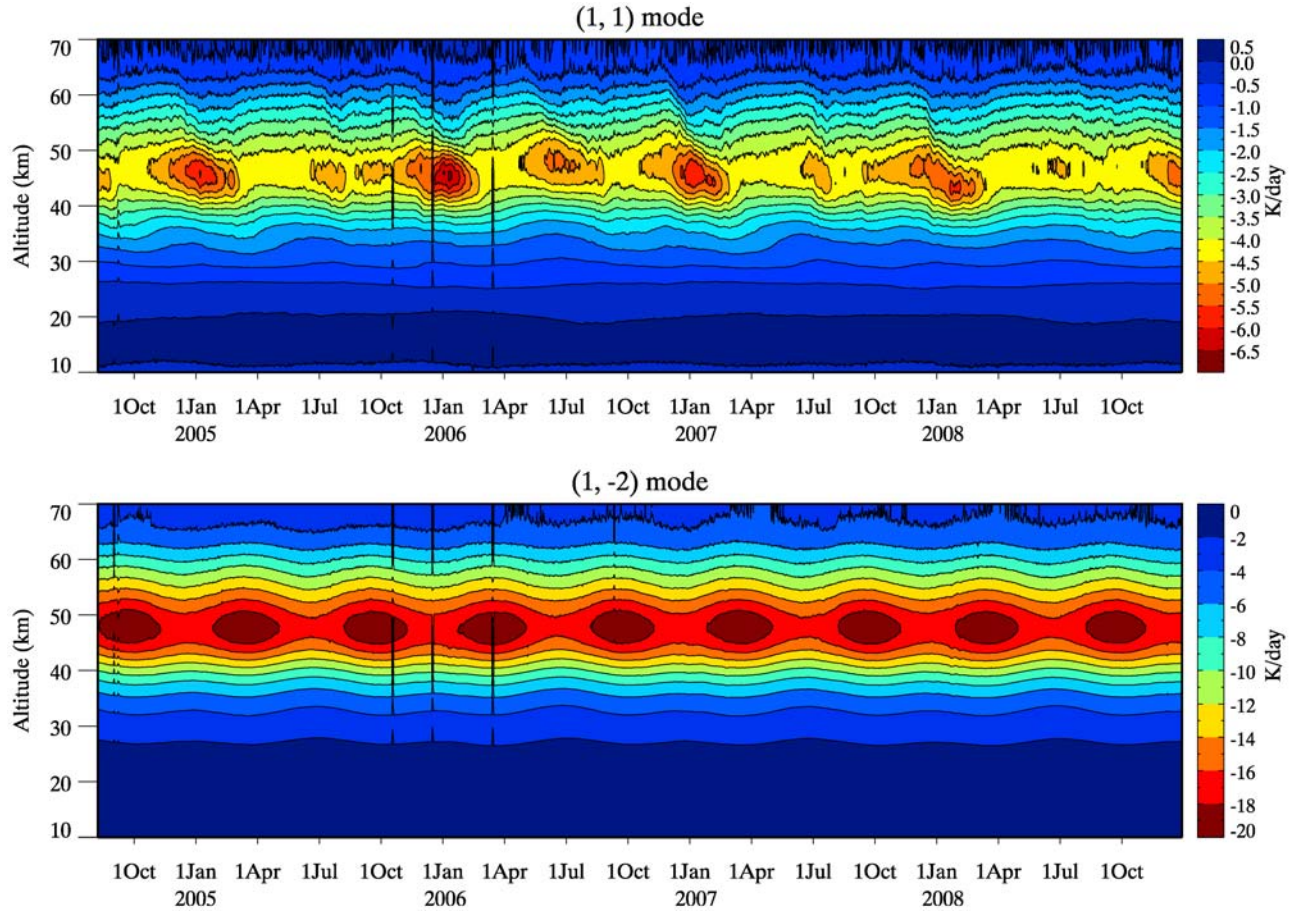


Figure 13. The seasonal variations of the coefficients of (top) diurnal Hough mode (1,1) $\alpha_{1,1}^c$ and (bottom) diurnal Hough mode (1,-2) $\alpha_{1,-2}^c$ in the heating rate (K/d) calculated from ozone observed by Aura/MLS.

mode is strongest near the December/January solstices and has secondary peaks near the June/July solstice. One interesting result is that the seasonal variation of the (1,1) propagating mode is out of phase with the seasonal variation of the diurnal tide in temperature, which has its maxima at the equinoxes [Xu *et al.*, 2009]. In contrast, the largest trapped mode (1,-2) is strong near the equinoxes.

[45] We can give a qualitative explanation for the seasonal variations in the dominant Hough modes. From Figure 5, we can see that the heating distribution is broader in latitude during equinox than during solstice. This is also apparent in Figure 6. This is primarily due to the decrease and eventual disappearance of the diurnal component of the heating at high latitudes during solstices as the day length becomes either very long (up to 24 h) or very short (eventually to zero). The heating that occurs at high latitudes in solstice will project more onto the daily mean and higher order components (semidiurnal, terdiurnal, etc.) and less onto the diurnal periodicity. Figure 4 shows that the latitude distribution of the (1,-2), (1,-1), and (1,-4) Hough modes are quite broad. These broad Hough modes dominate the decomposition of the heating rate in all seasons, but particularly at equinox when the heating itself is broadest. This explains why the trapped (1,-2) mode is strongest during equinoxes. From Figure 5, the magnitude of (1,-2) mode is -18.5 at day 80 and -15.8 at day 170. The magnitude of the

asymmetric (1,-1) mode increases to -2.44 at day 170 from almost zero at day 80. The projection of the (1,1) mode is better during solstices (magnitude -4.05) than during equinoxes (magnitude -3.95) because of the narrower latitudinal profile of the total diurnal heating (Figure 5).

5. Parameterization of the Diurnal Components in Ozone Heating

[46] The Aura/MLS observations provide a good opportunity for developing an observation-based parameterized description of the global heating rate due to ozone in which the seasonal variations are included. Such a parameterization could be used in tidal models that do not include interactive chemistry and therefore are not able to simulate the variations of this heating self-consistently. The inclusion of each individual Hough mode in the heating will facilitate investigation of the forcing of individual Hough modes in investigations of atmospheric tides. The atmosphere is a nonlinear system; the Hough mode decomposition of the heating allows for the model investigation of the dynamical coupling between the different Hough modes. With this application in mind, a new parameterized model of the ozone diurnal heating rate is developed and evaluated in this section.

[47] This parameterization of the ozone heating rate extends from pole to pole and from 10 km to 70 km in

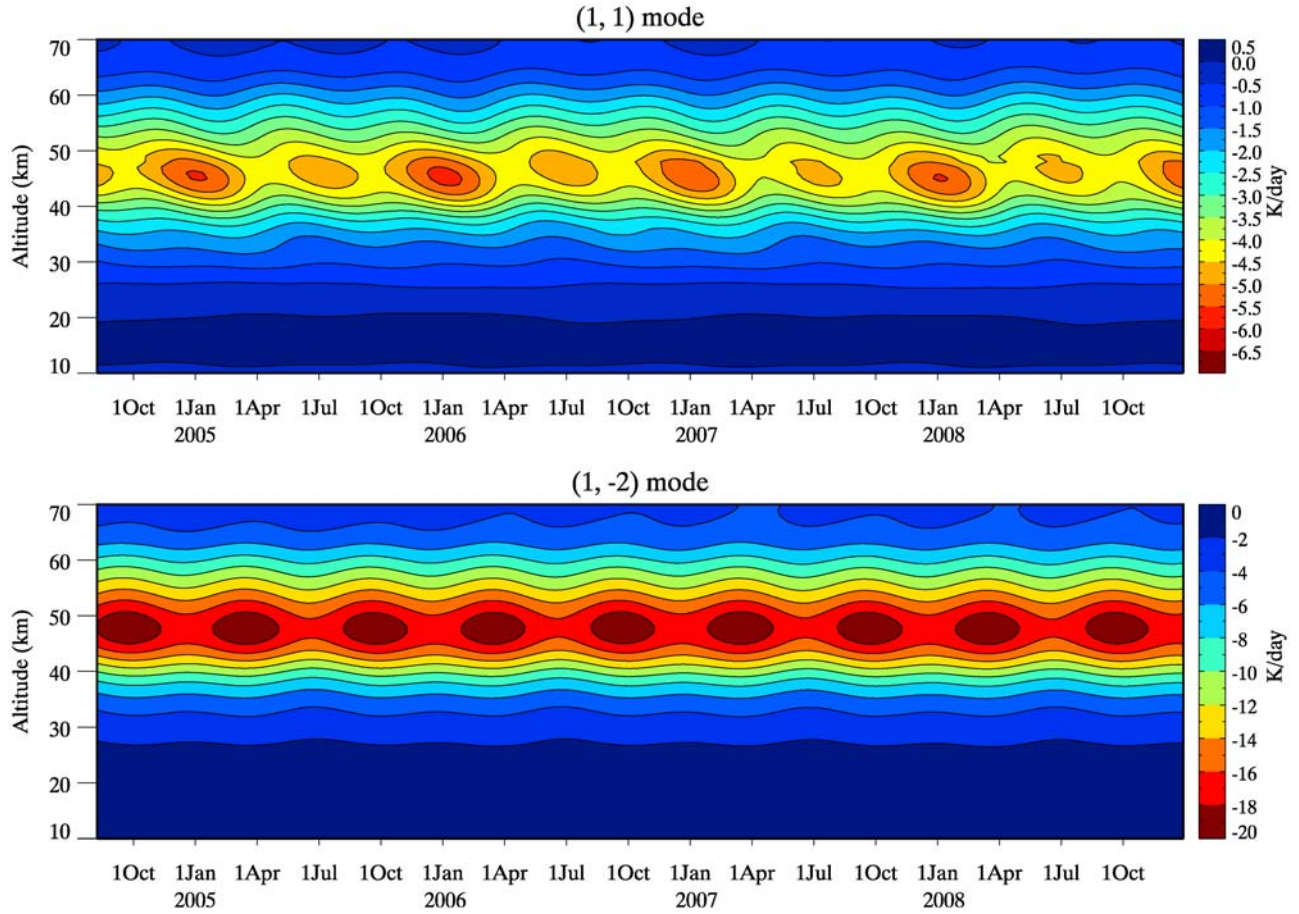


Figure 14. The same as Figure 13 but for the heating reconstructed from the parameterization model.

altitude. It can be used to reconstruct the ozone heating rate in each diurnal Hough mode and also to give the total diurnal component of the heating. The method for expanding the tabulated coefficients to get the latitudinal structure of the diurnal component of the ozone heating rate is described in section 3.2. The results are calculated in 1 km altitude increments from 10 km to 70 km.

[48] Rather than give the heating day by day, we use the seasonal analysis presented in section 4 to represent the variability. This reduces the variation to a manageable number of coefficients. The value of $|Q_1^c(d, \theta, z)|$ is much larger than $|Q_1^s(d, \theta, z)|$ and $|\alpha_{1,n}^c(d, z)| \gg |\alpha_{1,n}^s(d, z)|$ in equation (6). Neglecting $\alpha_{1,n}^s$, the total diurnal component in heating rate can be calculated by following formula:

$$q_1(d, \theta, z, t) = \sum_{n \neq 0} \left[\alpha_{1,n}^c(d, z) \cos(\omega_0 t) \right] \Theta_{1,n}(\theta)$$

$$\alpha_{1,n}^c = \bar{C}_n + C_{n,SAO} \cos \left[\frac{2\pi}{182.5(\text{day})} (d - d_{n,SAO}^c) \right] + C_{n,AO} \cos \left[\frac{2\pi}{365(\text{day})} (d - d_{n,AO}^c) \right] + C_{n,QBO} \cos \left[\frac{2\pi}{P_{n,QBO}(\text{day})} (d - d_{n,QBO}^c) \right]. \quad (9)$$

Additional information about the vertical distributions of \bar{C}_n , $C_{n,SAO}$, $d_{n,SAO}^c$, $C_{n,AO}$, $d_{n,AO}^c$, $P_{n,QBO}$, $C_{n,QBO}$, and $d_{n,QBO}^c$ is given in Data Sets S1–S16 in the auxiliary material that accompanies this paper.

[49] Now, we evaluate how well the variability can be reconstructed from the mean and the seasonal (SAO, AO, and QBO) fits. For comparison with Figure 13, Figure 14 gives the variability of the diurnal (1,1) and (1,–2) Hough modes reconstructed from the parameterized model. Comparison of Figure 13 and Figure 14 show that the parameterized model can reproduce the main features of the seasonal variability of the ozone heating rate.

[50] We also calculate the RMS difference between the parameterized model fit of the coefficient of the cosine term of each Hough mode and the daily heating rates. This gives the error associated with using the SAO, AO, etc. parameters to represent the seasonal cycle rather than using the daily calculated Hough mode values. Figure 15 shows vertical profiles of these RMS differences. Below 70 km, the deviations are small. For example, the maximum deviation for the (1,1) mode is about 0.23 K/d at the altitude of 47 km, while the average value in this mode at 47 km is –4.7 K/d; the relative deviation is 4.9%. The deviation of (1,–2) mode at 44 km is 0.43 K/d, but the average magnitude in this mode at 44 km is –15.8 K/d; the relative deviation is 2.7%.

6. Summary

[51] This paper calculates the Hough modes of the diurnal component of ozone heating and generates a parameterized representation for use in dynamical models. The heating is calculated from Aura/MLS ozone data using the heating

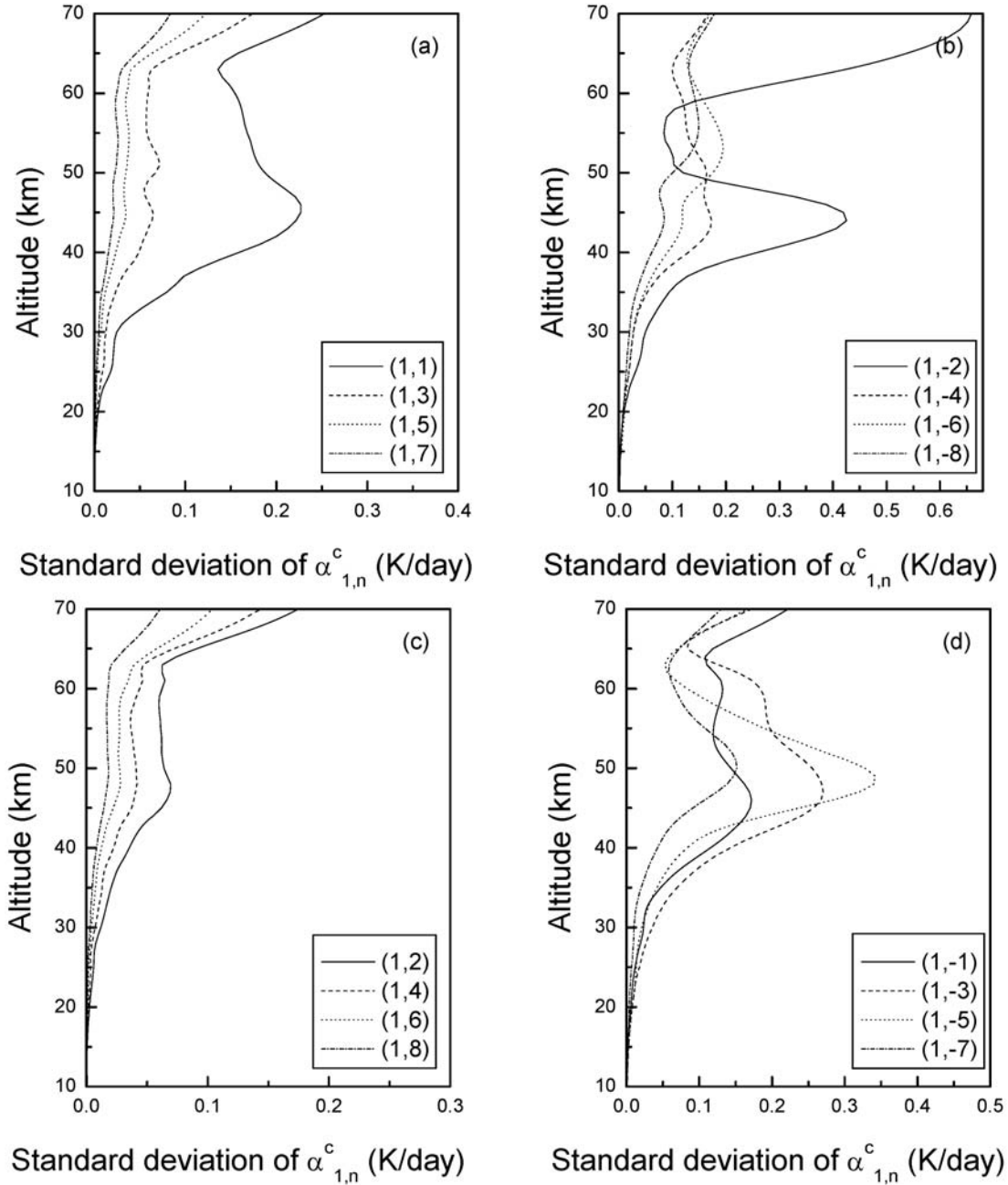


Figure 15. The RMS difference between the coefficient of the cosine term of each diurnal Hough mode reconstructed from the parameterization and the daily values.

parameterization of *Zhu* [1994], which is an update of an earlier calculation by *Strobel* [1978]. The parameterization converts absorbed solar energy to heat but does not include the chemical heating process that is important near the mesopause. As a first step, we use a time dependent photochemical model to evaluate the vertical range over which the Strobel/*Zhu* parameterization of ozone heating rate is valid. The results indicate that, in the mesopause region, the Strobel/*Zhu* parameterization model of ozone heating would overestimate the diurnal component in the heating rate because it does not include the chemical heating, which is strongest during night. Below 70 km, the parameterization can be used to determine the diurnal cycle in the heating rate.

[52] We use 4 years of continuous observations of the global distribution of atmospheric ozone observed by Aura/MLS to calculate the ozone heating rate and decompose the diurnal component of the heating into Hough modes. The results show that the largest component of the heating is the nonpropagating symmetric (1,-2) mode. The propagating (1,1) and nonpropagating (1,-4) symmetric modes have about equal strength, but with amplitudes from a quarter to one third of the (1,-2) heating rate, similar to the results of *Forbes* [1982] and *Groves* [1982].

[53] The mean and the annual (AO) and semiannual (SAO) periodicities of each diurnal Hough mode of ozone heating rate are presented. For the largest propagating mode

(1,1), there is an obvious SAO signature near 46 km that reaches a maximum near the equinoxes (see Figures 9a and 9b). Because the cosine of the diurnal heating is negative (the maximum heating is near noon), this means that the amplitude of the diurnal cycle in heating reaches minimum around equinoxes. There is also an AO in this mode near 40–50 km; the phase of the maximum is near solstice (see Figures 10a and 10b). The QBO amplitude of this mode is weak and the QBO phase has large variations near the peak of the heating rate of this mode.

[54] The trapped diurnal (1,–2) Hough mode is the strongest heating mode; it is 3–4 times larger than the (1,1) mode. This mode has an obvious SAO signature near 50 km and reaches maximum near solstice (see Figures 9c and 9d). The AO in this mode has maximum amplitude near 40 km; the phase there is near solstice (see Figures 10c and 10d). The AO is weaker than the SAO in the (1,–2) mode. The magnitude of the QBO variation in the (1,–2) mode is similar to that in the (1,1) mode. The strongest annual variation takes place in the (1,–1) mode; it reaches 3.6 K/d near 45 km, and the phase is at solstice (see Figures 11c and 11d).

[55] A new parameterization of the diurnal component of the ozone heating rate, which covers the vertical range of 10–70 km, is developed that includes the seasonal variations of each diurnal Hough mode of the heating. The model can be used to reconstruct the individual diurnal Hough modes for any day, latitude, and for altitudes from 10 to 70 km. The RMS differences between the reconstructed seasonal cycle and the daily heating rates are small. This parameterized model can provide a convenient tool for studying the diurnal tide. For example, it can be inserted into middle atmospheric numerical models that include dynamical interactions but where calculation of the photochemistry is not feasible in order to study the contributions of the ozone heating to forcing the diurnal tide and its seasonal variations. Additional applications are the investigation of the impact of forcing individual Hough modes on the tides and the interactions between different Hough modes.

[56] **Acknowledgments.** We thank the Jet Propulsion Laboratory MLS science team for retrieving and providing the Aura/MLS data. This research was supported by the National Science Foundation of China (40890165, 40874080, and 40921063) and the National Important Basic Research Project (2006CB806306). The project is also supported by the Specialized Research Fund for State Key Laboratories. The National Center for Atmospheric Research is sponsored by the National Science Foundation. Any opinions, findings, and conclusions or recommendations expressed in the publication are those of the authors and do not necessarily reflect the views of the National Science Foundation.

References

- Baldwin, M. P., et al. (2001), The quasi-biennial oscillation, *Rev. Geophys.*, 39(2), 179–229, doi:10.1029/1999RG000073.
- Brasseur, G., and D. Offermann (1986), Recombination of atomic oxygen near the mesopause: Interpretation of rocket data, *J. Geophys. Res.*, 91(D10), 10,818–10,824, doi:10.1029/JD091iD10p10818.
- Chapman, S., and R. S. Lindzen (1970), *Atmospheric Tides*, 200 pp., Springer, New York.
- Cunnold, D. M., W. P. Chu, R. A. Barnes, M. P. McCormick, and R. E. Veiga (1989), Validation Of SAGE II ozone measurements, *J. Geophys. Res.*, 94(D6), 8447–8460, doi:10.1029/JD094iD06p08447.
- Forbes, J. (1982), Atmospheric tides: 1. Model description and results for the solar diurnal component, *J. Geophys. Res.*, 87(A7), 5222–5240, doi:10.1029/JA087iA07p05222.
- Forbes, J. M. (1995), Tidal and planetary waves, in *The Upper Mesosphere and Lower Thermosphere: A Review of Experiment and Theory*, *Geophys. Monogr. Ser.*, vol. 87, edited by R. L. Johnson and T. L. Killeen, pp. 67–87, AGU, Washington, D. C.
- Forbes, J. M., and H. B. Garrett (1978), Thermal excitation of atmospheric tides due to insolation absorption by O_3 and H_2O , *Geophys. Res. Lett.*, 5, 1013–1016, doi:10.1029/GL005i012p01013.
- Forbes, J. M., and H. B. Garrett (1979), Theoretical studies of atmospheric tides, *Rev. Geophys.*, 17(8), 1951–1981, doi:10.1029/RG017i008p01951.
- Froidevaux, L., et al. (2008), Validation of Aura Microwave Limb Sounder stratospheric ozone measurements, *J. Geophys. Res.*, 113, D15S20, doi:10.1029/2007JD008771.
- Groves, G. V. (1982), Hough components of ozone heating, *J. Atmos. Terr. Phys.*, 44, 111–121, doi:10.1016/0021-9169(82)90114-3.
- Hagan, M. E. (1996), Comparative effects of migrating solar sources on tidal signatures in the middle and upper atmosphere, *J. Geophys. Res.*, 101(D16), 21,213–21,222, doi:10.1029/96JD01374.
- Hagan, M. E., J. M. Forbes, and F. Vial (1995), On modeling migrating solar tides, *Geophys. Res. Lett.*, 22, 893–896, doi:10.1029/95GL00783.
- Hagan, M. E., M. D. Burrage, J. M. Forbes, J. Hackney, W. J. Randel, and X. Zhang (1999), GSWM-98: Results for migrating solar tides, *J. Geophys. Res.*, 104(A4), 6813–6827, doi:10.1029/1998JA900125.
- Lacis, A. A., and J. E. Hansen (1974), A parameterization for the absorption of solar radiation in the Earth's atmosphere, *J. Atmos. Sci.*, 31, 118–133, doi:10.1175/1520-0469(1974)031<0118:APFTAO>2.0.CO;2.
- Mayr, H. G., and J. G. Mengel (2005), Interannual variations of the diurnal tide in the mesosphere generated by the quasi-biennial oscillation, *J. Geophys. Res.*, 110, D10111, doi:10.1029/2004JD005055.
- McLandress, C. (2002a), The seasonal variation of the propagating diurnal tide in the mesosphere and lower thermosphere. Part 1: The role of gravity waves and planetary waves, *J. Atmos. Sci.*, 59, 893–906, doi:10.1175/1520-0469(2002)059<0893:TSVOTP>2.0.CO;2.
- McLandress, C. (2002b), The seasonal variation of the propagating diurnal tide in the mesosphere and lower thermosphere. Part 2: The role of tidal heating and mean winds, *J. Atmos. Sci.*, 59, 907–922, doi:10.1175/1520-0469(2002)059<0907:TSVOTP>2.0.CO;2.
- Mlynczak, M. G., and S. Solomon (1993), A detailed evaluation of the heating efficiency in the middle atmosphere, *J. Geophys. Res.*, 98(D6), 10,517–10,541, doi:10.1029/93JD00315.
- Rong, P. P., J. M. Russell III, M. G. Mlynczak, E. E. Remsberg, B. T. Marshall, L. L. Gordley, and M. López-Puertas (2009), Validation of Thermosphere Ionosphere Mesosphere Energetics and Dynamics/Sounding of the Atmosphere using Broadband Emission Radiometry (TIMED/SABER) v1.07 ozone at 9.6 mm in altitude range 15–70 km, *J. Geophys. Res.*, 114, D04306, doi:10.1029/2008JD010073.
- Russell, J. M., III, L. L. Gordley, J. H. Park, S. R. Drayson, D. H. Hesketh, R. J. Cicerone, A. F. Tuck, J. E. Frederick, J. E. Harries, and P. J. Crutzen (1993), The Halogen Occultation Experiment, *J. Geophys. Res.*, 98(D6), 10,777–10,797, doi:10.1029/93JD00799.
- Strobel, D. F. (1978), Parameterization of the atmospheric heating rate from 15 to 120 km due to O_2 and O_3 absorption of solar radiation, *J. Geophys. Res.*, 83(C12), 6225–6230, doi:10.1029/JC083iC12p06225.
- Xu, J., Y. Wang, and Y. Wang (2000), The loss of photochemical heating caused by gravity waves in the mesopause region, *J. Atmos. Sol. Terr. Phys.*, 62, 37–45, doi:10.1016/S1364-6826(99)00091-7.
- Xu, J., A. K. Smith, and R. Ma (2003), A numerical study of the effect of gravity-wave propagation on minor species distributions in the mesopause region, *J. Geophys. Res.*, 108(D3), 4119, doi:10.1029/2001JD001570.
- Xu, J., A. K. Smith, W. Yuan, H.-L. Liu, Q. Wu, M. G. Mlynczak, and J. M. Russell III (2007), Global structure and long-term variations of zonal mean temperature observed by TIMED/SABER, *J. Geophys. Res.*, 112, D24106, doi:10.1029/2007JD008546.
- Xu, J., A. K. Smith, H.-L. Liu, W. Yuan, Q. Wu, G. Jiang, M. G. Mlynczak, J. M. Russell, and S. J. Franke (2009), Seasonal and quasi-biennial variations in the migrating diurnal tide observed by Thermosphere, Ionosphere, Mesosphere, Energetics and Dynamics (TIMED), *J. Geophys. Res.*, 114, D13107, doi:10.1029/2008JD011298.
- Zhu, X. (1994), An accurate and efficient radiation algorithm for middle atmosphere models, *J. Atmos. Sci.*, 51, 3593–3614, doi:10.1175/1520-0469(1994)051<3593:AAAERA>2.0.CO;2.

G. Jiang, J. Xu, and W. Yuan, State Key Laboratory of Space Weather, Center for Space Science and Applied Research, Chinese Academy of Sciences, PO Box 8701, Beijing 10091, China.

A. K. Smith, Atmospheric Chemistry Division, National Center for Atmospheric Research, PO Box 3000, Boulder, CO 80307-3000, USA. (aksmith@ucar.edu)